

The cytosolic carboxypeptidases CCP2 and CCP3 catalyze posttranslational removal of acidic amino acids

Olivia Tort, Sebastián Tanco, Cecilia Rocha, Ivan Bièche, Cecilia Seixas, Christophe Bosc, Annie Andrieux, Marie-Jo Moutin, Francesc Xavier Avilés, Julia Lorenzo, et al.

▶ **To cite this version:**

Olivia Tort, Sebastián Tanco, Cecilia Rocha, Ivan Bièche, Cecilia Seixas, et al.. The cytosolic carboxypeptidases CCP2 and CCP3 catalyze posttranslational removal of acidic amino acids. Molecular Biology of the Cell, 2014, 25 (19), pp.3017-27. 10.1091/mbc.E14-06-1072 . inserm-01116480

HAL Id: inserm-01116480
https://inserm.hal.science/inserm-01116480

Submitted on 13 Feb 2015

HAL is a multi-disciplinary open access archive for the deposit and dissemination of scientific research documents, whether they are published or not. The documents may come from teaching and research institutions in France or abroad, or from public or private research centers.

L'archive ouverte pluridisciplinaire **HAL**, est destinée au dépôt et à la diffusion de documents scientifiques de niveau recherche, publiés ou non, émanant des établissements d'enseignement et de recherche français ou étrangers, des laboratoires publics ou privés.

The cytosolic carboxypeptidases CCP2 and CCP3 catalyze posttranslational removal of acidic amino acids

Olivia Tort[a,b], Sebastián Tanco[a,c,d], Cecilia Rocha[b,e,f,g], Ivan Bièche[e,h], Cecilia Seixas[i], Christophe Bosc[j,k,l], Annie Andrieux[j,k,l], Marie-Jo Moutin[j,k,l], Francesc Xavier Avilés[a], Julia Lorenzo[a], and Carsten Janke[b,e,f,g]

[a]Institut de Biotecnologia i de Biomedicina, Department of Biochemistry and Molecular Biology, Universitat Autònoma de Barcelona, 08193 Bellaterra (Barcelona), Spain; [b]Institut Curie, 91405 Orsay, France; [c]Department of Medical Protein Research, VIB, 9000 Ghent, Belgium; [d]Department of Biochemistry, Ghent University, 9000 Ghent, Belgium; [e]PSL Research University, 75005 Paris, France; [f]Centre National de la Recherche Scientifique, UMR3306, 91405 Orsay, France; [g]Institut National de la Santé et de la Recherche Médicale, U1005, 91405 Orsay, France; [h]Department of Genetics, Institut Curie, 75248 Paris, France; [i]Centro de Estudos de Doenças Crónicas, Faculdade de Ciências Médicas, Universidade Nova de Lisboa, 1169-056 Lisbon, Portugal; [j]Institut des Neurosciences de Grenoble, Institut National de la Santé et de la Recherche Médicale, U836, CEA, Université Joseph Fourier, 38042 Grenoble, France; [k]Université Grenoble Alpes, 38000 Grenoble, France; [l]CEA, Institut de Recherches en Technologies et Sciences pour le Vivant, 38000 Grenoble, France

ABSTRACT **The posttranslational modification of carboxy-terminal tails of tubulin plays an important role in the regulation of the microtubule cytoskeleton. Enzymes responsible for deglutamylating tubulin have been discovered within a novel family of mammalian cytosolic carboxypeptidases. The discovery of these enzymes also revealed the existence of a range of other substrates that are enzymatically deglutamylated. Only four of six mammalian cytosolic carboxypeptidases had been enzymatically characterized. Here we complete the functional characterization of this protein family by demonstrating that CCP2 and CCP3 are deglutamylases, with CCP3 being able to hydrolyze aspartic acids with similar efficiency. Deaspartylation is a novel posttranslational modification that could, in conjunction with deglutamylation, broaden the range of potential substrates that undergo carboxy-terminal processing. In addition, we show that CCP2 and CCP3 are highly regulated proteins confined to ciliated tissues. The characterization of two novel enzymes for carboxy-terminal protein modification provides novel insights into the broadness of this barely studied process.**

Monitoring Editor
Stephen Doxsey
University of Massachusetts

Received: Jun 10, 2014
Revised: Jul 24, 2014
Accepted: Jul 24, 2014

INTRODUCTION

Microtubules (MTs) are dynamic, polarized polymers composed of α/β-tubulin heterodimers and constitute the largest filaments of the cytoskeleton (reviewed in Akhmanova and Steinmetz, 2008). MTs take part in a variety of cellular structures and functions in eukaryotic cells, such as cell shape and motility (reviewed in Etienne-Manneville, 2004), intracellular organization, and transport (reviewed in de Forges *et al.*, 2012). Moreover, MTs are the key structures of complex organelles such as centrioles (reviewed

This article was published online ahead of print in MBoC in Press (http://www.molbiolcell.org/cgi/doi/10.1091/mbc.E14-06-1072) on August 7, 2014.

O.T. performed and analyzed most of the experiments. S.T. participated in the molecular modeling, supervised some of the experiments, and participated in the writing of the manuscript. C.R. performed the ciliogenesis experiment and participated in the mouse line generation. I.B. performed the qRT-PCR analyses. C.S. performed initial deglycylase and cell culture experiments. C.B., A.A., and M.J.M. designed the CCP2- and CCP3-knockout mouse lines. O.T. and C.J. wrote the manuscript. The study was supervised by J.L., F.X.A., and C.J.

The authors declare no competing financial interests.

Address correspondence to: Julia Lorenzo (Julia.Lorenzo@uab.cat), Carsten Janke (Carsten.Janke@curie.fr).

Abbreviations used: Agbl, ATP/GTP binding protein–like; CPA, carboxypeptidase A; CCP, cytosolic carboxypeptidase; KO, knockout; MLCK, myosin light-chain kinase; MT, microtubule; PTM, posttranslational modification; TTLL, tubulin tyrosine ligase–like.

© 2014 Tort *et al*. This article is distributed by The American Society for Cell Biology under license from the author(s). Two months after publication it is available to the public under an Attribution–Noncommercial–Share Alike 3.0 Unported Creative Commons License (http://creativecommons.org/licenses/by-nc-sa/3.0).

"ASCB®," "The American Society for Cell Biology®," and "Molecular Biology of the Cell®" are registered trademarks of The American Society of Cell Biology.

Supplemental Material can be found at:
http://www.molbiolcell.org/content/suppl/2014/08/04/mbc.E14-06-1072.DC1.html

in Bornens, 2012) and axonemes, which are the backbones of cilia and flagella (reviewed in Jana *et al.*, 2014).

Considering the huge variety of MT functions, the targeting of distinct MTs for precisely defined roles in cells appears primordial. Functionally distinct MT species can be generated by either incorporating selected tubulin isotypes into the MT lattice (reviewed in Ludueña and Banerjee, 2008) or generating posttranslational modifications (PTMs) onto selected MTs in cells (reviewed in Janke and Bulinski, 2011). Most of the known PTMs of tubulin take place at the C-terminal tails of tubulins, which are the key interaction sites for microtubule-associated proteins (MAPs) and motors (Sirajuddin *et al.*, 2014). PTMs of these tails include polyglutamylation (Eddé *et al.*, 1990), polyglycylation (Redeker *et al.*, 1994), detyrosination/tyrosination (Arce *et al.*, 1975; Hallak *et al.*, 1977; Thompson, 1977), and generation of Δ2-tubulin (Paturle-Lafanechère *et al.*, 1991).

Enzymes catalyzing polyglutamylation, polyglycylation, and tyrosination are members of the tubulin tyrosine ligase–like (TTLL) family (Ersfeld *et al.*, 1993; Janke *et al.*, 2005; Ikegami *et al.*, 2006; Ikegami and Setou, 2009; van Dijk *et al.*, 2007; Wloga *et al.*, 2008; Rogowski *et al.*, 2009). So far, only deglutamylases have been identified in the family of cytosolic carboxypeptidases (CCPs), a subfamily of M14 metallocarboxypeptidases (Kalinina *et al.*, 2007; Rodriguez de la Vega *et al.*, 2007; Kimura *et al.*, 2010; Rogowski *et al.*, 2010). Four of six mammalian CCP enzymes catalyze deglutamylation and Δ2-tubulin generation; however, the function of the remaining two enzymes has remained elusive (Rogowski *et al.*, 2010; Berezniuk *et al.*, 2013). Of importance, not only tubulin is modified by CCPs; some proteins with gene-encoded acidic C-terminals appear to be cleaved in vivo, such as myosin light-chain kinase and telokin (Rogowski *et al.*, 2010).

Using structural modeling and enzymatic assays, we find that CCP2 and CCP3 are carboxypeptidases that specifically hydrolyze acidic amino acids. We further characterize the activities of these enzymes with chimeric substrates, and through the study of the individual knockout and double-knockout mice. Our work on CCP2 and CCP3 completes the functional characterization of the CCP family and suggests an important functional role of this enzyme family in posttranslational protein regulation. Moreover, our study demonstrates that the as-yet-undiscovered tubulin-modifying enzymes for deglycylation and detyrosination are not found within the CCP family.

RESULTS

Prediction of substrate specificities for CCP2 and CCP3

After the discovery that four (CCP1, CCP4, CCP5, CCP6) of the six murine CCPs are deglutamylases (Rogowski *et al.*, 2010), attention turned to the potential functions of CCP2 and CCP3. Considering that enzymes for deglycylation and detyrosination of tubulin have not been identified so far and that the reverse enzymes for these two reactions are all members of the same TTLL family, one expectation was that CCP2 and CCP3 could be involved in either or both of these PTMs. Indeed, an initial report (Sahab *et al.*, 2011) attributed a detyrosinating activity to CCP2; however, unambiguous evidence for this activity was not provided, and overexpression of CCP2 did not lead to a strong increase in detyrosinated tubulin. To gain more insight into the substrate preferences of CCP2 and CCP3, we modeled the catalytic domains of the two enzymes based on the CCP crystal structures of *Pseudomonas aeruginosa* (PDB 4a37; Otero *et al.*, 2012), *Burkholderia mallei* (PDB 3k2k), and *Shewanella denitrificans* (PDB 3l2n; Figure 1A and Supplemental Figure S1A).

The pockets or subsites of the carboxypeptidases, which are the binding sites of their substrates, are usually designated using a standard nomenclature (Schechter and Berger, 1967). Accordingly, substrate residues are indicated as –P3–P2–P1↓P1′, where P1′ is the C-terminal substrate residue to be cleaved, and the corresponding binding subsites in the carboxypeptidase are named S3, S2, S1, and S1′ (Figure 1B). In the structural models of hCCP2 and hCCP3, an arginine (Arg) at position 255 (numbering according to active bovine carboxypeptidase A1 [CPA1; PDB 3HLP]), at the base of the S1′ subsite or specificity pocket, appears to be critical in determining the substrate preference of these enzymes (Figure 1A). In metallocarboxypeptidases, the residue at position 255 directly interacts with the C-terminal side chain of the substrates (reviewed in Arolas *et al.*, 2007; Fernández *et al.*, 2010). A basic amino acid in this position suggest that hCCP2 and hCCP3 should have a preference for acidic amino acids, similar to carboxypeptidase O (Wei *et al.*, 2002; Lyons and Fricker, 2011). Sequence alignment of human and murine CCPs predicts that Arg-255 is conserved in all six CCPs (Supplemental Figure S1B). Moreover, a lysine or arginine (Lys/Arg-250) close to Arg-255 is also conserved in the specificity pocket of CCPs and may contribute to their preference for acidic amino acids (Figure 1A and Supplemental Figure S1B).

In the hCCP2 and hCCP3 models, the entrance to the active site presents an extended positively charged area, which is similarly formed by conserved residues throughout all CCPs and can be associated with different binding subsites of these enzymes (Figure 1C and Supplemental Figure S1C). The positively charged area around the active site of CCPs explains their preference for substrates with long polyglutamate chains, such as polyglutamylated tubulin (Rogowski *et al.*, 2010; Berezniuk *et al.*, 2012; Wu *et al.*, 2012). In particular, positively charged amino acids in the S1 subsite are consistent with binding of glutamic acids present at the P1 position of deTyr-tubulin. In addition, the hCCP2/3 models show positively charged S2 and S3 subsites, which can explain the ability of these enzymes to accommodate long acidic chains such as lateral polyglutamylation (Figure 1C).

The overlap of the structural models of hCCP3 and hCCP2 shows that the main determinants of substrate binding are conserved (Figure 1D and Supplemental Figure S1B), and sequence alignments extend these conclusions to the entire murine and human CCP family (Supplemental Figure S1, B and C). Thus the structure of the active site of CCPs reveals that the entire family has a preference for cleaving acidic amino acids. The modeling further helped us to determine the controversial identity of the specificity-determining residue corresponding to position 255 of bovine CPA in the CCPs (Kalinina *et al.*, 2007; Rodriguez de la Vega *et al.*, 2007) as being arginine (Figure 1A).

CCP2 and CCP3 generate Δ2-tubulin in cells

Deglutamylation can occur on the C-terminally exposed, gene-encoded glutamate residues of proteins, such as detyrosinated tubulin and myosin light-chain kinase (MLCK), or on posttranslationally added polyglutamate chains. This activity was demonstrated for CCP1, CCP4, and CCP6; however, no activity had been detected for CCP2 and CCP3 (Rogowski *et al.*, 2010). One of the potential reasons for the absence of measurable activity of these two enzymes was the difficulty of expressing these proteins in cell lines. To overcome this problem, we included a synthetic, codon-optimized cDNA of mouse CCP3 (Uniprot Q8CDP0-1), as well as a short human CCP3 isoform (Uniprot Q8NEM8-2), in our study, and we expressed yellow fluorescent protein (YFP)/green fluorescent protein (GFP) fusion proteins in HEK293T cells for 40 h instead of 24 h to increase expression levels.

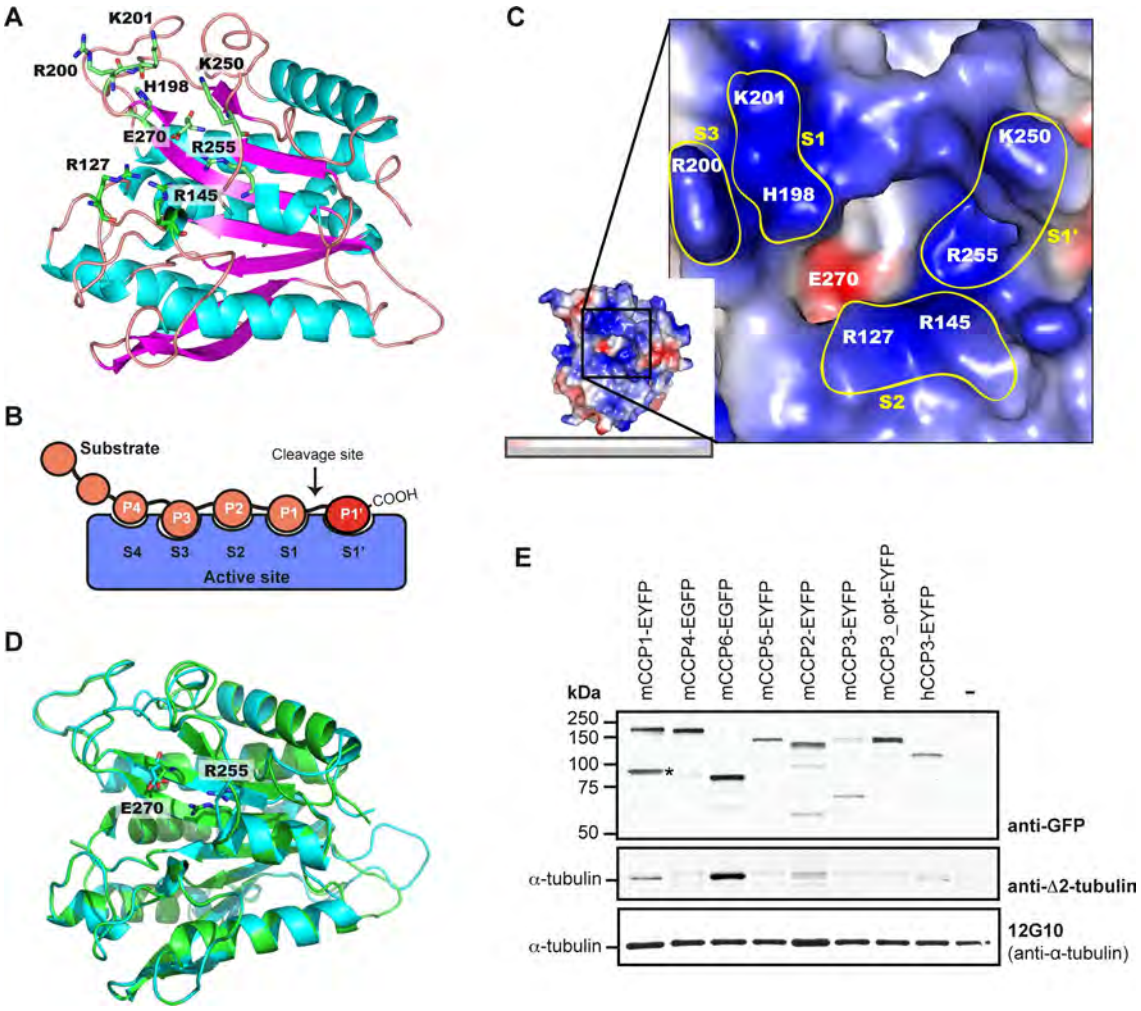
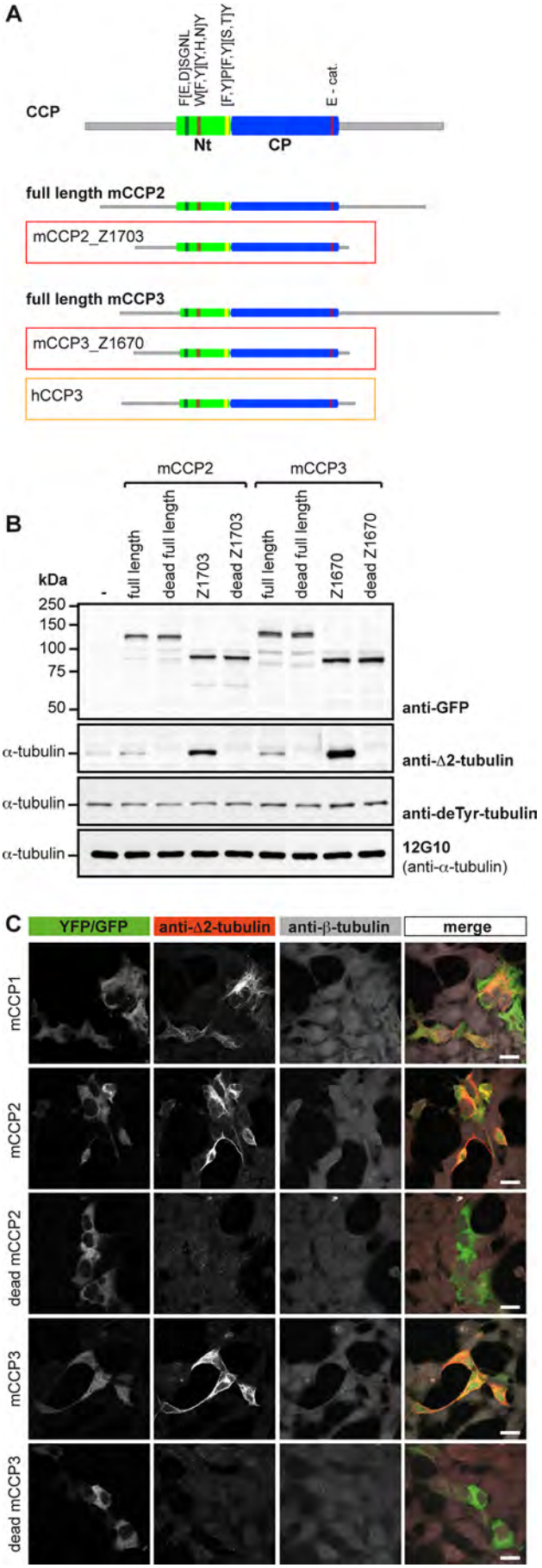


FIGURE 1: Structural modeling of the carboxypeptidase domains of CCP2 and CCP3. (A) Modeled structure of human CCP3 (as a convention, all residues are numbered according to the corresponding active-site residues in bovine carboxypeptidase A1 after propeptide cleavage). The catalytic E270, the main substrate-specificity determining R255, and putative secondary binding-site residues are indicated. (B) Scheme of the substrate-binding subsites in the active site of carboxypeptidases (Schechter and Berger, 1967). (C) Vacuum electrostatics surface representation of the active site of hCCP3. Basic residues are indicated in blue and acidic residues in red. Positions 198 and 201 (corresponding to H462 and K465 in hCCP3) shape the S1 binding site in the hCCP3 model. Positions 127 and 145 (R414 and R424 in hCCP3) define the S2 subsite. Position 200 (R464 in hCCP3) is oriented toward the outer part of the active site, possibly defining an additional, positively charged S3 subsite. Note that although S1′ is defined by different residues (Supplemental Figure S1B), we here only depicted positions 250 and 255 because they are the major determinants of substrate specificity for CCPs. (D) Overlapped model structures of hCCP2 (cyan) and hCCP3 (green) demonstrate the conserved positions in the active-site residues (key residues E270 and R255 are shown). (E) Immunoblots of extracts of HEK293T cells expressing YFP-tagged murine and human CCP proteins. Expression of YFP-CCPs was analyzed with anti-GFP, and deglutamylating activity was visualized with anti–Δ2-tubulin labeling on endogenous α-tubulin. α-Tubulin levels were controlled with 12G10 antibody. mCCP3_opt is a codon-optimized synthetic gene construct; hCCP3 is the human 73-kDa isoform of CCP3 (Q8NEM8-2 Uniprot). Note the presence of a specific degradation product (*) of mCCP1. Images of structures in A, C, and D were generated with PyMOL 1.3. (–), control without transfection.

After 40 h of expression, the cells were lysed and protein extracts analyzed by immunoblotting. As expected, CCP6 and CCP1 overexpression led to a marked increase in Δ2-tubulin, pointing to them as the most active deglutamylases (Δ2-tubulin is barely detectable in these cells, and thus increased levels indicate deglutamylating activity; Figure 1E). A very weak signal of Δ2-tubulin was detected after overexpression of CCP2, but no clear Δ2-tubulin signal was seen after expression of full-length, codon-optimized murine CCP3. Strikingly, human CCP3 generated a slight increase in the Δ2-tubulin signal (Figure 1E). The simplest explanation is that the 73-kDa human CCP3 isoform we used was shorter than the 116-kDa murine CCP3 and thus might be more active in cells, analogous to what we previously observed for truncated glutamylase enzymes from the TTLL family (van Dijk *et al.*, 2007; Rogowski *et al.*, 2009).

We thus generated a series of truncated forms of murine CCP2 and CCP3 in order to determine the minimal active size of these enzymes (Supplemental Table S1). The YFP-tagged truncated forms were expressed in HEK293T cells, and their activity was assessed by immunoblot for Δ2-tubulin (Supplemental Figure S2, A and B).



Indeed, the truncated versions of both murine CCP2 and CCP3 showed a clear Δ2-tubulin–generating activity, demonstrating that both can act as deglutamylating enzymes. The shortest and most active versions are CCP2_Z1703 and CCP3_Z1670 (Figure 2A), which were obtained by truncating nonconserved N- and C-terminal sequences to obtain 65-kDa proteins that were similar in size and domain structure to the highly active deglutamylase CCP6 (Figure 2B and Supplemental Figure S2). Immunocytochemical analysis of HEK293T cells expressing CCP2 and CCP3 further showed a specific Δ2-tubulin labeling associated with the MTs in YFP-positive cells (Figure 2C). To demonstrate that the observed Δ2-tubulin generation after CCP2 and CCP3 expression is directly catalyzed by their active carboxypeptidase (CP) domains, we generated enzymatically dead versions by mutating the essential catalytic residues Glu-593 in mouse CCP2 and Glu-540 in mouse CCP3 (Glu-270 in bovine CPA and Glu-1094 in mouse CCP1; Wu *et al.*, 2012). Enzymatically dead mutants of full-length and truncated versions of CCP2 and CCP3 were expressed at similar levels as the active forms but did not generate Δ2-tubulin (Figure 2B). Strikingly, a very faint Δ2-tubulin band present in the control cells is now absent in the cells overexpressing the enzymatically dead enzymes (Figure 2B), suggesting that these enzymes can act as dominant negative competitors for endogenous enzymes. These experiments demonstrate that the enzymatic activity of CCP2 and CCP3 is involved in the observed deglutamylation reactions on tubulin, leading to Δ2-tubulin.

CCP2 was previously suggested to have a detyrosinating activity (Sahab *et al.*, 2011). Although comparison of active sites of CCPs with CPA, an enzyme that specifically hydrolyzes Tyr from C-terminal positions (Argaraña *et al.*, 1980), strongly suggested that CCPs cannot catalyze Tyr hydrolysis (Figure 1), we still tested this possibility experimentally. We used the detyr-tubulin antibody to specifically detect the generation of detyrosinated tubulin in HEK293T cell extracts overexpressing the optimized forms of CCP2 and CCP3. No detectable differences were observed in detyrosinated tubulin, whereas the increase of Δ2-tubulin signal clearly indicated the activity of the overexpressed enzymes (Figure 2B). Thus CCP2 and CCP3 are not involved in the detyrosination of tubulin, and the identity of

FIGURE 2: Optimized forms of mCCP2 and mCCP3 reveal deglutamylating activity. (A) Scheme of generic CCP; full-length and truncated forms of mCCP2 and mCCP3, and the 73-kDa hCCP3 isoform. The green boxes indicate in the conserved N-terminal domain (Nt) specific to CCPs, with FESGNL, WYYY, and YPYTY conserved motifs (Rodriguez de la Vega *et al*, 2007). The blue box shows the conserved carboxypeptidase domain (CP) with the catalytic residue E270 (E-cat). Gray lines are nonconserved sequences that were partially truncated in the optimization. The shortest truncated versions that are still enzymatically active are mCCP2_Z1703 and mCCP3_Z1670 (red boxes). They are shown in comparison to the full-length versions and to hCCP3 (orange box). (B) Immunoblot of cell extracts from HEK293T cells expressing YFP-tagged, full-length mCCP2 and mCCP3, their optimized truncated forms (A), and enzymatically dead versions as controls. Δ2-Tubulin was used as readout for deglutamylating activity. Detyrosination and deglutamylase activities were followed by generation of deTyr- and Δ2-tubulin. Active enzymes generate Δ2-tubulin. (C) Immunocytochemistry of HEK293T cells transfected with active and inactive truncated YFP-tagged mCCP2 and mCCP3, as well as with GFP-mCCP1. After fixation of the cells with a protocol preserving microtubule structures (Bell and Safiejko-Mroczka, 1995), Δ2-tubulin was detected. Images were collected on an inverted confocal microscope (Leica SP5; Leica, Wetzlar, Germany) using a 63× objective at 25°C and analyzed with LAF AS Lite 1.8.1 (Leica). Scale bar, 20 μm.

these long-sought enzymes (Argaraña *et al.*, 1978) remains a conundrum.

Enzymatic specificities of CCP2 and CCP3

To further characterize whether CCP2 and CCP3 can remove subsequent glutamate residues from longer stretches of glutamates, such as those generated by enzymatic polyglutamylation (Audebert *et al.*, 1993; van Dijk *et al.*, 2007) or genetically encoded as in the case of MLCK, we used C-terminally engineered chimeras of telokin, a short version of MLCK, which is one of the few known substrates of CCP1 (Rogowski *et al.*, 2010). Truncated active versions of CCP2 and CCP3 were coexpressed in HEK293T cells together with different C-terminal variants of YFP-telokin. The deglutamylation (removal for long glutamate chains) was monitored using the polyE antibody in immunoblot analysis (Shang, 2002), and the final deglutamylation product (ending with only one glutamate) was detected with the anti–Δ2-tubulin antibody (Figure 3A). Both CCP2_Z1703 and CCP3_Z1670 were able to trim long (7-Glu) and shorter polyglutamate chains from the C-terminus of chimeric telokin, as shown by decreased polyE signals and increased Δ2-tubulin immunoreactivity (Figure 3B). CCP1, known to shorten long glutamate chains, was used as positive control.

According to the predictions from the molecular modeling (Figure 1), any negatively charged amino acid would be susceptible to be cleaved by CCPs, not only glutamic acids. However, the previously tested CCP1, CCP4, and CCP6 where shown to specifically remove glutamate in the conditions applied previously (Rogowski *et al.*, 2010). To test the specificity of CCP2 and CCP3, we coexpressed them with telokin variants exposing either one or two aspartic acids at their C-termini. CCP1 and CCP2 generated weak anti–Δ2-tubulin–reactive bands at ~55 kDa, indicative of a cleavage of aspartate; however, much stronger Δ2 signals were obtained when chimeric telokins with C-terminal glutamates were expressed (Figure 3B and Supplemental Figure S3A). In contrast to CCP1 and CCP2, CCP3 converted both aspartate- and glutamate-ending telokin variants to their Δ2 form, and as judged from the intensity of the Δ2 signal, with a similar preference (Figure 3B and Supplemental Figure S3A). It is most likely that the weak Δ2 signal generated from telokin-Asp by CCP1 and CCP2 shows that these two enzymes can cleave aspartate; however, this activity might require high enzyme concentrations, as even after 40 h of overexpression it was less efficient than glutamate hydrolysis. In cells in which endogenous levels of CCP1 and CCP2 are much lower than with the overexpression situation, both enzymes might preferentially or even exclusively hydrolyze glutamate. In contrast, CCP3 shows no obvious enzymatic preference for either glutamate or aspartate removal and might thus be involved in protein deaspartylation in cells.

To check the potential effect of the novel enzymatic activity on the functional broadness of enzymatic C-terminal degradation of proteins on a proteome level, we compared the number of proteins with C-terminal poly-Glu stretches, which can be substrates of deglutamylases (Rogowski *et al.*, 2010), with the number of acidic C-terminal tails including Asp residues. We restricted our analysis to the four very well annotated proteomes of *Homo sapiens*, *Mus musculus*, *Drosophila melanogaster*, and *Caenorhabditis elegans*. Three main conclusions can be drawn from the numbers we obtained (Figure 3C and Supplemental Table S3). First, the presence of a putative deaspartylating activity (CCP3 and possibly other CCPs under specific conditions) strongly increases the number of proteins that could be C-terminally modified by the CCP family. Second, the number of proteins with acidic C-terminal stretches is much higher in the mouse and human than in *D. melanogaster* and *C. elegans*. This could indicate a greater need for this regulatory mechanism in more complex organisms, which is also underlined by the greater number of CCP genes in mice and humans than in *D. melanogaster* and *C. elegans*. Finally, it is not clear whether deaspartylation activity can be found in the last two invertebrates, as clear homologues of CCP3 have not been identified. It thus appears that the discovery of a deaspartylating activity could have a significant impact on the functional reach of C-terminal degradation and offer novel evolutionary insight into the development of this PTM.

Glycylation is a posttranslational modification similar to polyglutamylation, performed by members of the TTLL family (Rogowski *et al.*, 2009). Nothing is known about the enzymes responsible for shortening or removing posttranslationally generated glycine chains from tubulin. The unique deglycylase identified so far is an M20 peptidase family member in *Giardia duodenalis* (Lalle *et al.*, 2011). Because this enzyme deglycylates the 14-3-3 proteins, and because M20 peptidases are not found in the mammalian genome, other candidates were considered as potential deglyclases in mammals, among them CCP2 and CCP3. Glycylation is typically enriched on the axonemes of motile cilia and flagella (Redeker *et al.*, 1994). Thus the presence of CCP2 and CCP3 genes in ciliated organisms (Rodríguez de la Vega Otazo *et al.*, 2013) and their increased expression levels in mouse tissues with motile cilia such as testis and trachea (Figure 4A) provided a potential link to glycylation. Although the structural model already suggested that both enzymes are rather specific to acidic amino acids (Figure 1), we wanted to obtain additional experimental proof to confirm this. Our attempts to directly test deglycylating activity in cells with glycylated MTs, which could be generated by expression of glycylating enzymes, failed due to the toxicity of this treatment for the cells. Thus we developed an alternative test for deglycylating activity, in which we coexpressed a chimeric telokin containing four Gly residues on the very C-terminus. This construct is specifically detected with the polyclonal antibody polyG, and removal of only one Gly residue completely abolished detection (Supplemental Figure S3B). The chimeric telokin-Gly was coexpressed together with CCP2_Z1703 or CCP3_Z1670, and a similar experiment was performed with a polyE antibody and a telokin with three Glu residues as positive control (Supplemental Figure S3C). Whereas both CCP2_Z1703 and CCP3_Z1670 were perfectly able to remove C-terminal glutamates, the unchanged polyG signals strongly suggest that C-terminally located Gly residues cannot be hydrolyzed by these enzymes. Thus CCP2 and CCP3 do not carry an intrinsic deglycylase activity.

Expression and potential functional roles of CCP2 and CCP3 in ciliated cells

Having demonstrated that all members of the CCP family are deglutamylating enzymes, we wanted to gain more insight into their specific functions on the whole-organism level. We thus quantified the relative expression levels of all six CCP family members by quantitative real-time-PCR (qRT-PCR) with cDNA samples prepared from a representative range of organs. Although qRT-PCR data are semiquantitative, it was obvious that both CCP2 and CCP3 are expressed at relatively low levels in most organs (Figure 4A), especially when compared with CCP1 (Supplemental Figure S4A). CCP4, in contrast, was barely detectable in a range of organs, suggesting a very specialized function in the subgroup of organs where it is expressed (Supplemental Figure S4A). The expression profiles of CCP2 and CCP3 are highly similar; both enzymes are predominantly found in the testis, trachea, and lung, all tissues containing cells with motile cilia (Figure 4A). In two tissues, retina and adipose tissue, CCP3 was relatively strongly expressed, whereas CCP2 was barely detected (Figure 4A; Kalinina *et al.*, 2007).

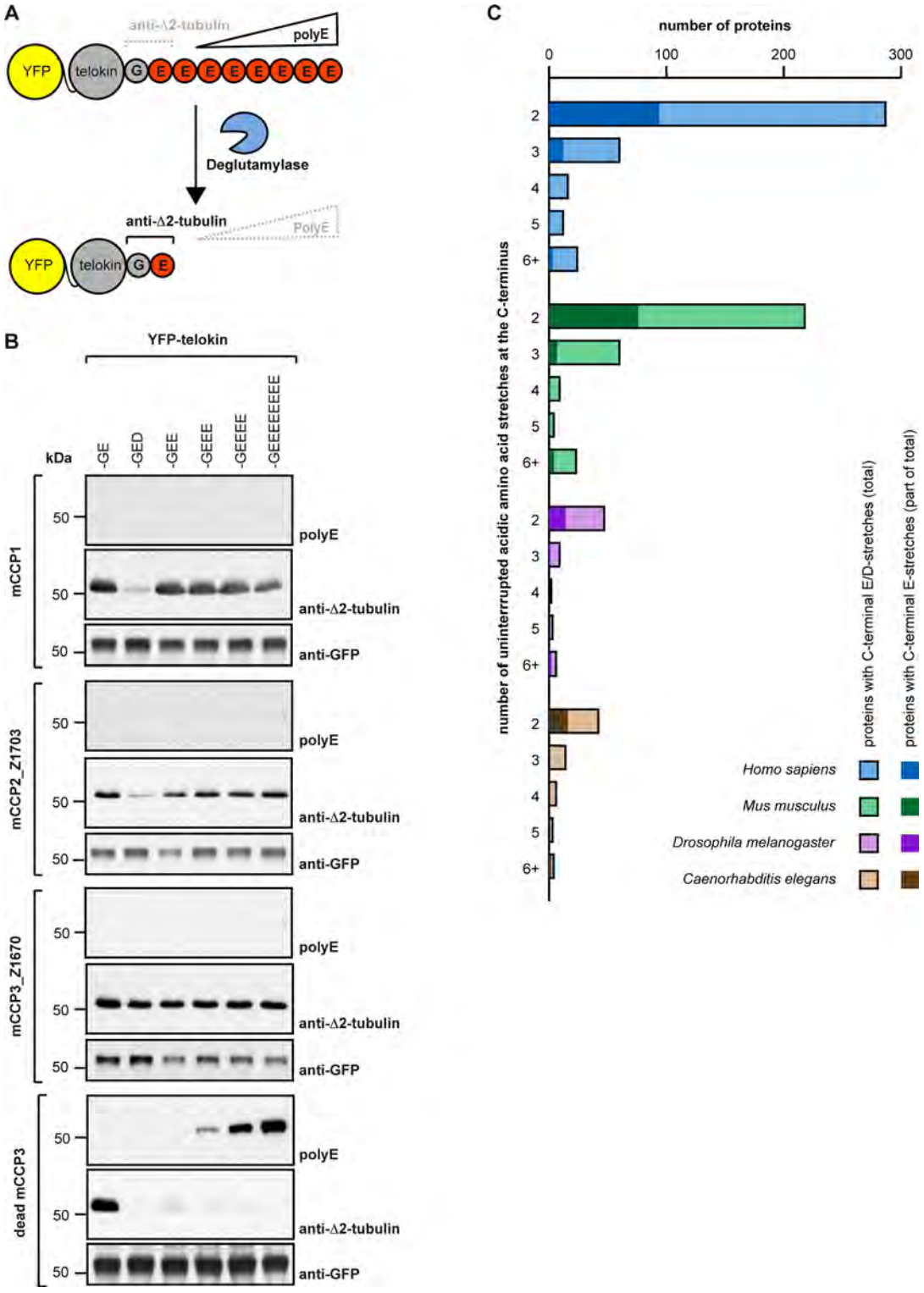


FIGURE 3: Substrate specificity of mCCP2 and mCCP3. (A) Schematic representation of the experimental setup. PolyE antibody recognizes telokin constructs with three or more consecutive C-terminal glutamate residues, whereas anti-Δ2-tubulin antibody detects specifically the C-terminal –GE epitope. C-terminal degradation is detected by generation of the Δ2-tubulin epitope, and absence or strong decrease of the polyE signal on telokin (Rogowski *et al*, 2010). (B) Immunoblot analysis of HEK293T extracts after coexpression of different YFP-CCPs and YFP-telokin variants. Activity is monitored as shown in A. The activity of truncated mCCP2 and mCCP3 (Figure 2A) is tested with telokin variants with different numbers of consecutive glutamate residues to test processivity and with an aspartate residue to test specificity. The activities are compared with mCCP1, an established deglutamylase (Rogowski *et al*, 2010), and a dead version of mCCP3 as negative control. Note that only mCCP3 removes aspartate efficiently. (C) Bioinformatic analysis of the number of proteins with uninterrupted C-terminal acid sequence stretches. Each column represents the total number of proteins per category (mixed Asp and Glu stretches), and the darker insets represent uninterrupted Glu stretches.

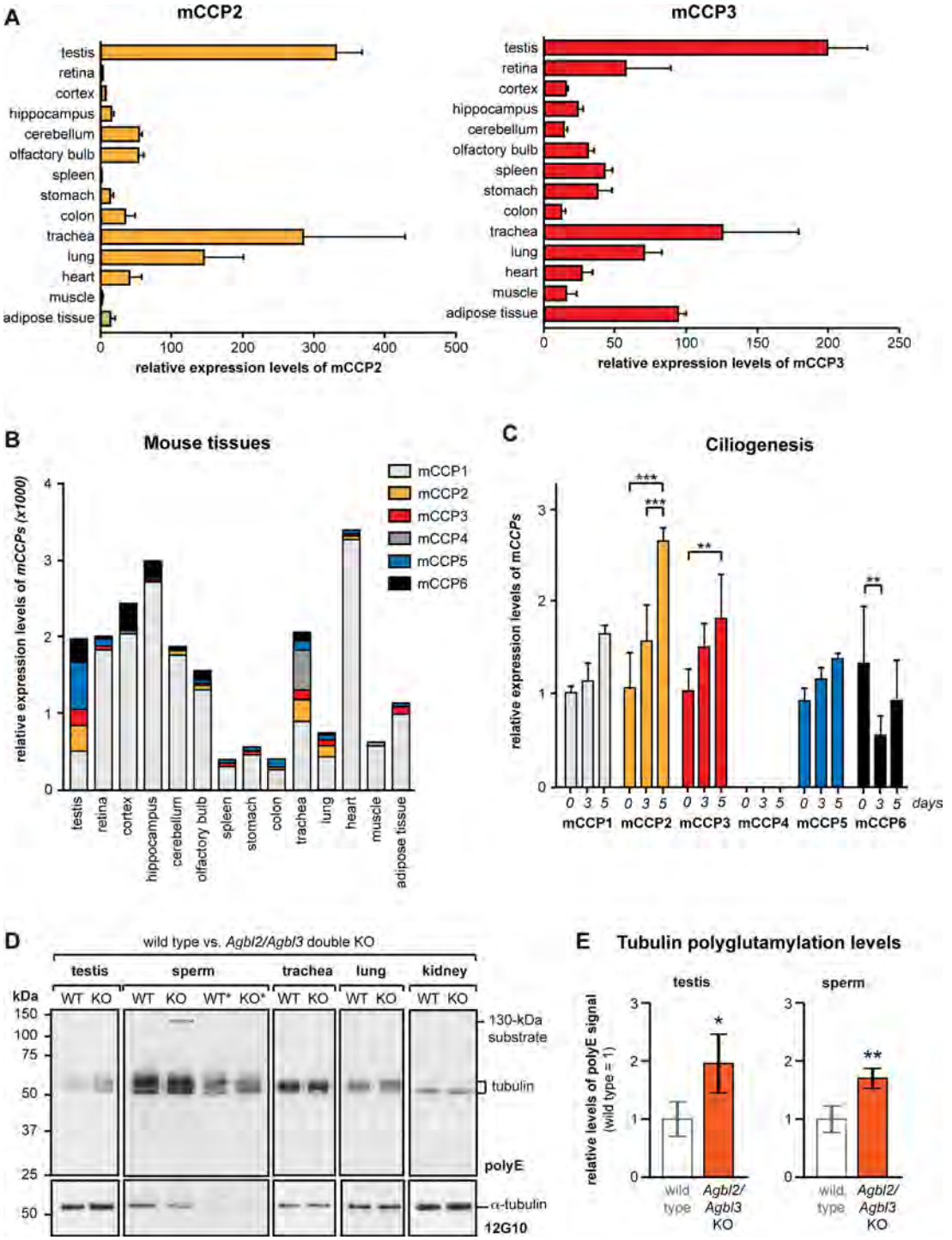


FIGURE 4: Analysis of mCCP2 and mCCP3 expression and of the *Agbl2/Agbl3* double-KO mice. (A) Relative expression levels of mCCP2 and mCCP3 in different organs of wild-type (WT) mice as determined by qRT-PCR. Average values relative to the *Tbp* gene expression are represented, and error bars represent SD of five independent experiments. (B) Cumulative view of the relative expression levels of all six CCP genes in different murine tissues (values from A and Supplemental Figure S4A). (C) qRT-PCR analysis of expression levels of all six *CCP* genes during ciliogenesis in cultured IMCD3 cells. Cells were serum starved and analyzed at 0, 3, and 5 d after starvation. Mean values of expression levels relative to *Tbp* expression and relative to 0 d from three to five independent experiments are shown; error bars show SD. Two-way analysis of variance was used to determine significance levels (**$p < 0.01$; ***$p < 0.001$). (D) Comparative immunoblot analysis of protein extracts from different organs of WT and *Agbl2/Agbl3* double-KO mice with polyE. Total tubulin levels were detected with anti–α-tubulin antibody (12G10). For sperm that showed the highest polyE levels in the tubulin region, the experiment was repeated with half of the initial protein load (lanes labeled with ⋆). (E) Quantitative analysis of the polyE signal relative to the 12G10 signal *Agbl2/Agbl3* double-KO mice relative to WT. Four of each WT and double KO were analyzed (Supplemental Figure S5), and relative values were plotted (WT was set to 1); error bars show SD. Student's *t* test was used to determine significance levels (*$p < 0.05$; **$p < 0.01$).

On comparison of the relative expression levels of the CCP enzymes as determined by qRT-PCR, it is obvious that CCP1 is the deglutamylase with the highest expression levels and the broadest distribution in different tissues (Figure 4B). Although this does not allow judging the functional importance of those enzymes, it suggests that CCP1 catalyzes a large share of deglutamylation reactions. Indeed, the knockout model for CCP1, the Purkinje cell degeneration (*pcd*) mouse, shows severe defects related to tubulin hyperglutamylation in several organs (Rogowski *et al.*, 2010). In contrast, other CCP enzymes might have more specialized functions in specific cells, organelles, or even on some selected MTs within cells.

The elevated expression levels of CCP2 and CCP3 in ciliated tissues containing axonemes, such as the testis, lung, and trachea, suggest a potential role of these enzymes in the assembly or function of cilia. To investigate this link, we quantified the expression of all six CCPs during ciliogenesis in IMCD3 cells in culture by qRT-PCR at 0, 3, and 5 d after induction of ciliogenesis by serum starvation. Apart from CCP4, all other CCPs could be detected, but only CCP2 and CCP3 show a statistically significant increase of expression levels during ciliogenesis (Figure 4C). Thus several enzymes of the deglutamylase family are likely to be involved in ciliary outgrowth, maintenance, and function, consistent with the importance of glutamylation in cilia assembly and function (Bosch Grau *et al.*, 2013; Pathak *et al.*, 2014); however, CCP2 and CCP3 are likely to play highly specific role in these processes.

The similar expression profiles of CCP2 and CCP3 determined by qRT-PCR and previously by in situ hybridization (Rodríguez de la Vega Otazo *et al.*, 2013) suggest some functional overlap of these two enzymes. Because the individual knockout (KO) mouse models for CCP2 (*Agbl2* [ATP/GTP binding protein–like]) and CCP3 (*Agbl3*) are both fertile, we generated double (*Agbl2/Agbl3*) KO mice. These mice were viable and displayed no obvious phenotypic alterations. To study the potential change in polyglutamylation levels on tubulin and other proteins, we dissected selected organs, prepared tissue extracts, and analyzed them with polyE antibody in immunoblot (Figure 4D and Supplemental Figures S4B and S5). Compared to wild-type mice, tubulin polyglutamylation was increased in the testes and sperm of the *Agbl2/Agbl3* double-knockout mice (Figure 4E and Supplemental Figure S5). Apart from testes and sperm, no other organ showed detectable changes in tubulin polyglutamylation levels in *Agbl2/Agbl3* KO mice (Figures 4D). In addition to tubulin, polyE immunoreactivity of a 130-kDa protein was increased in sperm of a 5-wk-old *Agbl2/Agbl3* KO mice; however, this band was not detected in the 4-mo-old mice. In the previous analysis of the *pcd* mouse, the 130-kDa substrate was identified as MLCK1, of which the C-terminal glutamate stretch is detected with polyE (Rogowski *et al.*, 2010). Our observations in the *Agbl2/Agbl3* KO mice indicate that CCP2 and CCP3 are complementarily involved in the deglutamylation of MLCK1 in sperm, but that other enzymes could compensate for the absence of these two enzymes in adult mice (Figure 4D and Supplemental Figure S5). A similar increase in polyE immunoreactivity of MLCK1 was observed in stomach of the *Agbl2* KO mice, as well as in stomach and oviduct of the *Agbl3* KO mice (Supplemental Figure S4B). These data show that in certain organs, CCP2, CCP3, or both enzymes are involved in the deglutamylation of MLCK1 (Supplemental Figure S4B and 4D). However, no visible phenotype has been related to this change in deglutamylation in these mice, perhaps due to compensation during development.

DISCUSSION

Protein PTMs consisting of the ligation or hydrolysis of amino acids have recently been attributed an increasing range of functions, and the discovery of enzymes involved in polyglutamylation, polyglycylation, or detyrosination/tyrosination have opened new opportunities for mechanistic and functional studies. Amino acid ligases for Glu, Gly, or Tyr have been identified in the conserved TTLL family. Enzymes removing Glu residues from protein C-termini were found within the newly discovered CCP family (reviewed in Janke and Bulinski, 2011). Initially, these discoveries raised hopes that the remaining enzymes, such as detyrosinases or deglycylases, are also members of the CCP family (Sahab *et al.*, 2011). The goal of the present study was to determine unambiguously the enzymatic specificity of the remaining two members of the mammalian CCP family, CCP2 and CCP3.

The reason that CCP2 and CCP3 had not been analyzed with the same rigorousness as the other members of the family (Rogowski *et al.*, 2010) was mainly related to the difficulties in expressing these proteins, which hampered the development of enzymatic assays. The availability of the crystal structure of a CCP (Otero *et al.*, 2012) allowed us to generate a structural model of CCP2 and CCP3, on the basis of which we predicted the acidic substrate specificity of these two enzymes. Guided by these predictions and optimizing the coding sequences of CCP2 and CCP3 led us to the demonstration that both enzymes are consistent with C-terminal deglutamylation activity on proteins, similar to the family members CCP1, CCP4, and CCP6 (Rogowski *et al.*, 2010). On the level of MTs, CCP2 and CCP3 can generate Δ2-tubulin, and their ability to shorten long Glu chains also allows them to deglutamylate laterally polyglutamylated tubulin. Δ2-Tubulin, as well as polyglutamylated forms of tubulin, is specifically accumulated on neuronal, centriolar, ciliary, and flagellar MTs (Paturle-Lafanechère *et al.*, 1994; Ikegami and Sato, 2010; Vogel *et al.*, 2010; Bosch Grau *et al.*, 2013). Thus the specific expression of CCP2 and CCP3 in ciliated tissues, as well as the increase of their expression levels during ciliogenesis, suggest that they fulfill specific functions in the regulation of the two PTMs in these organelles. Indeed, we showed that double knockout of both enzymes in mice results in significant changes in tubulin polyglutamylation in testes and sperm, which is consistent with the relatively high expression levels of CCP2 and CCP3 in testes. However, similar changes could not be visualized in other ciliated tissues of these mice.

Our results show that CCP2 and CCP3 participate in the process of deglutamylation; however, other enzymes, such as CCP1, CCP4, and CCP6, are also involved and might in most cases compensate for the absence of these two enzymes. It is thus possible that CCP2 and CCP3 play some highly regulated, specific roles in adjusting tubulin modifications locally or temporally in most cells and organs. This could be important for fine-tuning specific MT functions but does not induce global changes visible on the level of the whole tubulin pool. The absence of strong phenotypic alterations in *Agbl2/Agbl3* double-KO mice also points toward highly specified functions that might only be revealed under specific conditions, such as adaptation to evolutionary pressure or diseases. We recently made a similar observation for a member of the TTLL family (Rocha *et al.*, 2014).

Analyzing the enzymatic activities of CCP3 further revealed that this particular enzyme can, besides Glu, also hydrolyze Asp residues from C-terminal positions. CCP3 seems to catalyze Glu and Asp removal with equal efficiency, whereas all other enzymes of the CCP family show only weak activity for Asp. It might thus be that Asp hydrolysis is an important function for CCPs, but apart from CCP3, other CCPs require specific cofactors or other regulatory events to efficiently catalyze this reaction. The biological effect of this novel enzymatic activity could be significant. In addition to modifying

proteins with C-terminally exposed Glu residues, such as MLCK1 or telokin (Rogowski *et al.*, 2010), we now envisage differential C-terminal modification of a larger range of potential substrates. The possibility to selectively remove the Glu and the Asp residues by different CCPs opens the possibility that this novel PTM has a broader effect on protein functions than initially expected from deglutamylation alone. Still, the absence of striking phenotypic alterations of the *Agbl3* (CCP3) knockout mouse indicates that these modifications can be redundantly performed or have only fine-regulatory roles that remain to be discovered.

In summary, we showed that all members of the murine CCP family are involved in protein deglutamylation, and we further discovered a novel deaspartylating activity for CCP3. Our functional analyses suggest that CCP2 and CCP3 fulfill complementary functions in regulating protein glutamylation in ciliated cells and tissues. Strikingly, the deletion of both enzymes in mice did not impede key organism functions, which indicates that, similar to other enzymes involved in this type of PTM, the two CCPs might play roles in fine-tuning protein functions. The analysis of the enzymatic activities of CCP2 and CCP3 completes the repertoire of enzymes involved in ligation and removal of acidic amino acids on proteins. The discovery of a novel Asp-hydrolyzing activity further expands the complexity of this type of PTM, broadens the range of potential substrates, and points toward novel functions of the CCP enzyme family.

MATERIALS AND METHODS

Structural alignment

The catalytic domain of CCP3 was modeled with the help of the RaptorX server (Källberg *et al.*, 2012) and using as templates the available structures of three CCPs from *P. aeruginosa* (PDB 4a37; Otero *et al.*, 2012), *B. mallei* (PDB 3k2k), and *S. denitrificans* (PDB 3l2n). Ramachandran plots were derived for the proposed models to verify proper stereochemistry of the residues, and local and overall model quality was verified using Verify3D (Bowie *et al.*, 1990; Luthy *et al.*, 1992) and Prosa-web (Sippl, 1993; Wiederstein and Sippl, 2007). Arg at position 255 was supported by the structure-based sequence alignment performed by RaptorX, I-TASSER (Zhang, 2008; Roy *et al.*, 2010), GalaxyWEB (Ko *et al.*, 2012), and PDBsum (Laskowski, 2001; unpublished data).

Cell culturing, transfection, and immunoblotting

Adherent HEK293T cells were maintained under standard conditions and transfected (see Supplemental Table S1 for plasmids) with linear polyethylenimine (PEI; Polysciences, Eppelheim, Germany) in a 1:3 DNA:PEI ratio. Cells were collected after 48 h, lysed in 100 mM Tris-HCl, pH 8, 150 mM NaCl, and 0.1% NP-40 supplemented with 1/1000 of the EDTA-free protease inhibitor cocktail Set III (Calbiochem, Darmstadt, Germany), and centrifuged for 10 min, 15,000 × *g* at 4°C. SDS–PAGE and immunoblotting onto nitrocellulose membranes (EMD Millipore, Darmstadt, Germany) were performed using standard protocols. Proteins were detected using different primary antibodies (Supplemental Table S2) and visualized with horseradish peroxidase–labeled secondary antibodies, followed by chemiluminescence (ECL Western blot detection kit; GE Healthcare, Velizy-Villacoublay, France).

Cell fixation and immunocytochemistry

For immunofluorescence, HEK293T cells were seeded onto culture dishes and transfected 24 h after plating, as described before. After 12 h, cells were trypsinized and plated onto sterile glass coverslips in six-well plates (Nunc, Villebon sur Yvette, France) and incubated for 24 h before fixation. A fixation method to preserve microtubule structures was applied (Bell and Safiejko-Mroczka, 1995). In brief, cells were incubated 10 min at room temperature in 1 mM dithiobis(succinimidyl propionate) (DSP; Thermo Scientific, Rockford, IL) in Hanks' balanced salt solution, followed by 10 min of incubation with 1 mM DSP in microtubule-stabilizing buffer (MTSB). Cells were washed in phosphate-buffered saline (PBS) for 5 min with 0.5% Triton X-100 (Fluka, Saint-Quentin Fallavier, France) in MTSB before fixation with 4% paraformaldehyde (PFA) in MTBS. This step was followed by a 5-min wash in PBS, 5 min in 100 mM glycine in PBS, and a final wash in PBS.

After fixation, cells were washed for 5 min in PBS containing 0.1% Triton X-100 and then incubated with primary antibodies in PBS, 0.1% Triton X-100, and 2% bovine serum albumin (Sigma-Aldrich, Villebon sur Yvette, France) for 1 h at room temperature. Next cells were washed four times with PBS and 0.1% Triton X-100, followed by 1-h incubation with anti–rabbit Alexa Fluor 568 and anti–mouse Alexa Fluor 350 (Invitrogen, Saint Aubin, France) in PBS and 0.1% Triton X-100. Washes were performed before coverslips were mounted with ProLong Gold (Life Technologies, Saint Aubin, France).

RNA extraction and quantitative PCR

Organs were dissected from 4- to 5-wk-old mice and immediately frozen in liquid nitrogen. IMCD3 cells were maintained under standard conditions and serum starved for 3 and 5 d to induce ciliogenesis. RNA extraction was performed using TRIzol reagent (Life Technologies), following manufacturer's instructions. The RNA concentration and quality was determined, and qRT-PCR was applied under standard conditions using the SYBR Green Master Mix kit on the ABI Prism 7900 Sequence Detection System (PerkinElmer-Cetus, Courtaboeuf, France) using specific primers (Supplemental Table S4).

Search in the database for proteins ending with acidic amino acidic stretches

A bioinformatic search for proteins susceptible to be substrates of CCPs was performed using ScanProsite tool (de Castro *et al.*, 2006). The search for total acidic proteins was performed using the pattern [ED](*n*)>, where *n* represents the number of consecutive acidic residues at the protein's C-terminus. We searched for C-terminal stretches from two and longer. The total number of proteins with a given number of acidic amino acids at the C-terminus was determined from the *H. sapiens*, *M. musculus*, *D. melanogaster*, and *C. elegans* taxons of the 2014_05 UniProtKB/Swiss-Prot database, using the default settings. Splice variants were not allowed. The same search was repeated for C-terminal tails containing only glutamate residues.

Generation of *Agbl2* KO, *Agbl3* KO, and *Agbl2*/*Agbl3* double-KO mice

The conditional mutant mouse lines for *Agbl2* (on exon 9) and for *Agbl3* (on exons 7 + 8) were established at the Mouse Clinical Institute (MCI, Illkirch, France). The targeting vector was constructed as follows. The 5′ (4.5 kb for *Agbl2*; 3.5 kb for *Agbl3*), 3′ (3.5 kb for CCP2; 4.7 kb for CCP3), and inter-loxP (1.1 kb for *Agbl2*; 3.0 kb for *Agbl3*) fragments were PCR amplified and sequentially subcloned into an MCI proprietary vector containing the LoxP sites and a Neo cassette flanked by Flippase Recognition Target sites (Supplemental Figure S6). The linearized construct was electroporated in 129S2/SvPas mouse embryonic stem (ES) cells. After selection, targeted clones were identified by PCR using external primers and further confirmed by Southern blot with 5′ and 3′ external probes. Two positive ES clones were injected into blastocysts, and derived male

chimeras gave germline transmission. The excision of the neomycin-resistance cassette was performed in vivo by breeding the chimeras with a Flp deleter line (C57BL/6N genetic background FLP under ACTB promoter). The Flp transgene was segregated by breeding the first germline mice with a wild-type C57BL/6N animal. For generation of *Agbl2* KO and *Agbl3* KO mice, *Agbl2* and *Agbl3* floxed mice were crossed with transgenic mice expressing Cre recombinase under the control of a cytomegalovirus promoter.

The *Agbl2/Agbl3* double-KO mice were then generated by crossing the single-KO mice. Genomic DNA isolated from mouse-tail snip was analyzed by PCR.

Mice were genotyped by PCR according to MCI protocols using GoTag polymerase (Promega, Charbonnieres, France) and 33 amplification cycles. The following sets of three primer pairs were used to define the genotypes.

For CCP2:

1) CCP2_Ef: CATCCTTAGCAACTCTCCCGATGCCC, CCP2_Er: GGTGGGGGTGTGTGTGAAATGGCTG
2) CCP2_Lf: CCACGAGCGACCTTCCAAACCTACC, CCP2_Lr: AGCTGCCTGCTACAGCAAACGGG
3) CCP2_Lf: CCACGAGCGACCTTCCAAACCTACC, CCP2_Er: GGTGGGGGTGTGTGTGAAATGGCTG

For CCP3:

1) CCP3_Ef: CCTCAAAACCACTGACCATCTAGACAGCC, CCP3_Er: GGGCTGGAGTAGACACTGTACATAAGAAAGC
2) CCP3_Lf: CTGGAGTGGGACTAGTATCTTGAAGATGGG, CCP3_Lr: CCCCAGGAACTTTGACCCTTTGTGTGC
3) CCP3_Lf: CTGGAGTGGGACTAGTATCTTGAAGATGGG, CCP3_Er: GGGCTGGAGTAGACACTGTACATAAGAAAGC

Animal experimentation

Wild-type C57BL/6N, *Agbl2* KO, *Agbl3* KO, and *Agbl2/Agbl3* double-KO mice were housed under specific-pathogen-free conditions in the animal facility of the Institut Curie. Animals were maintained with access to food and water ad libitum in a colony room kept at constant temperature (19–22°C) and humidity (40–50%) at 12-h light/dark cycles. All experimental procedures were performed in strict accordance with the guidelines of the European Community (86/609/EEC) and the French National Committee (87/848) for care and use of laboratory animals.

ACKNOWLEDGMENTS

We thank S. Bronsoms and S. A. Trejo (Servei de Proteòmica i Biologia Estructural, Universitat Autònoma de Barcelona) and S. Vacher (Institut Curie) for technical support and discussion; and F. Cortés and M. Costa (Servei de Cultius Cellulars, Producció d'Anticossos i Citometria [SCAC], Universitat Autònoma de Barcelona), M. Vendrell and M. Roldán (Servei de Microscopia, Universitat Autònoma de Barcelona), C. Alberti, E. Belloir, Y. Bourgeois, V. Dangles-Marie, I. Grandjean, and A. Thadal (Institut Curie Animal Facility), L. Papon (Institut de Génétique Moléculaire de Montpellier, Montpellier, France), S. Leboucher (Institut Curie Histology Facility), C. Lasgi (Institut Curie Flow Cytometry Facility), C. Eponina (Instituto de Biologia, Rio de Janeiro, Brazil), and S. Geimer (Universität Bayreuth, Bayreuth, Germany) for technical assistance. We are grateful to T. Giordano, M. M. Magiera, P. Marques, and N.-L. J. Nguyen (Institut Curie) and F. Amargant and A. Otero (Institut de Biotecnologia i de Biomedicina; IBB) for excellent guidance and experimental support and to J. Souphron and A. M. Wehenkel (Institut Curie) for instructive discussions. We thank the Institut Clinique de la Souris (Institut Génétique Biologie Moléculaire Cellulaire, Strasbourg, France) for generating the *Agbl2*- and *Agbl3*-knockout mice. This work was supported by Spanish Ministry of Science and Innovation Grant BIO2013-44973-R; the Network of Excellence of the Generalitat de Catalunya (SGR; Spain); a Predoctoral Contract for Training in Health Research (PFIS) grant from Instituto Carlos III; an EMBO short-term fellowship (ASTF 45-2014); the Institut Curie, Centre National de la Recherche Scientifique, Institut National de la Santé et de la Recherche Médicale, and Fondation Pierre-Gilles de Gennes 3T grant (C.J.); FRM Grant FDT20120925331 (C.R.); a Fundação para a Ciência e a Tecnologia postdoctoral grant (A.C.S.); French National Research Agency (ANR) Awards ANR-12-BSV2-0007, ANR-10-LBX-0038, and part of ANR-10-IDEX-0001-02 PSL (C.J.); INCA Grant 2009-1-PLBIO-12-IC (C.J.); ARC Program SL220120605303 (C.J.); the EMBO Young Investigators Programme (C.J.); Project Tyr-TIPs-ANR-07-BLAN-0045 (A.A.); ARC Grant SFI20111204053 (M.J.M.); and a grant of La Ligue contre le Cancer comité de Savoie (M.J.M.).

REFERENCES

Akhmanova A, Steinmetz MO (2008). Tracking the ends: a dynamic protein network controls the fate of microtubule tips. Nat Rev Mol Cell Biol 9, 309–322.

Arce CA, Rodriguez JA, Barra HS, Caputo R (1975). Incorporation of L-tyrosine, L-phenylalanine and L-3,4-dihydroxyphenylalanine as single units into rat brain tubulin. Eur J Biochem 59, 145–149.

Argaraña CE, Barra HS, Caputto R (1978). Release of tyrosine from tubulinyl-tyrosine by brain extract. Separation of a carboxypeptidase from tubulin-tyrosine ligase. Mol Cell Biochem 19, 17–21.

Argaraña CE, Barra HS, Caputto R (1980). Tubulinyl-tyrosine carboxypeptidase from chicken brain: properties and partial purification. J Neurochem 34, 114–118.

Arolas JL, Vendrell J, Aviles FX, Fricker LD (2007). Metallocarboxypeptidases: emerging drug targets in biomedicine. Curr Pharm Des 13, 347–364.

Audebert S, Desbruyères E, Gruszczynski C, Koulakoff A, Gros F, Denoulet P, Eddé B (1993). Reversible polyglutamylation of alpha- and beta-tubulin and microtubule dynamics in mouse brain neurons. Mol Biol Cell 4, 615–626.

Bell PJ, Safiejko-Mroczka B (1995). Improved methods for preserving macromolecular structures and visualizing them by fluorescence and scanning electron microscopy. Scanning Microsc 9, 843–857; discussion, 858–860.

Berezniuk I, Lyons PJ, Sironi JJ, Xiao H, Setou M, Angeletti RH, Ikegami K, Fricker LD (2013). Cytosolic carboxypeptidase 5 removes α- and γ-linked glutamates from tubulin. J Biol Chem 288, 30445–30453.

Berezniuk I, Vu HT, Lyons PJ, Sironi JJ, Xiao H, Burd B, Setou M, Angeletti RH, Ikegami K, Fricker LD (2012). Cytosolic carboxypeptidase 1 is involved in processing α- and β-tubulin. J Biol Chem 287, 6503–6517.

Bornens M (2012). The centrosome in cells and organisms. Science 335, 422–426.

Bosch Grau M, Gonzalez Curto G, Rocha C, Magiera MM, Marques Sousa P, Giordano T, Spassky N, Janke C (2013). Tubulin glycylases and glutamylases have distinct functions in stabilization and motility of ependymal cilia. J Cell Biol 202, 441–451.

Bowie JU, Ltcy R, Eisenberg D (1990). A method to identify protein sequences that fold into a known three-dimensional structure. Science 253, 164–170.

De Castro E, Sigrist CJa, Gattiker A, Bulliard V, Langendijk-Genevaux PS, Gasteiger E, Bairoch A, Hulo N (2006). ScanProsite: detection of PROSITE signature matches and ProRule-associated functional and structural residues in proteins. Nucleic Acids Res 34, W362–W365.

De Forges H, Bouissou A, Perez F (2012). Interplay between microtubule dynamics and intracellular organization. Int J Biochem Cell Biol 44, 266–274.

Eddé B, Rossier J, Le Caer JP, Desbruyères E, Gros F, Denoulet P (1990). Posttranslational glutamylation of alpha-tubulin. Science 247, 83–85.

Ersfeld K, Wehland J, Plessmann U, Dodemont H, Gerke V, Weber K (1993). Characterization of the tubulin-tyrosine ligase. J Cell Biol 120, 725–732.

Etienne-Manneville S (2004). Actin and microtubules in cell motility: which one is in control? Traffic 5, 470–477.
Fernández D, Boix E, Pallarès I, Avilés FX, Vendrell J (2010). Analysis of a new crystal form of procarboxypeptidase B: further insights into the catalytic mechanism. Biopolymers 93, 178–185.
Hallak M, Rodriguez J, Barra H, Caputto R (1977). Release of tyrosine from tyrosinated tubulin. Some common factors that affect this process and the assembly of tubulin. FEBS Lett 73, 147–150.
Ikegami K, Mukai M, Tsuchida J, Heier RL, Macgregor GR, Setou M (2006). TTLL7 is a mammalian β-tubulin polyglutamylase required for growth of MAP2-positive neurites. J Biol Chem 281, 30707–30716.
Ikegami K, Sato S (2010). Tubulin polyglutamylation is essential for airway ciliary function through the regulation of beating asymmetry. Proc Natl Acad Sci USA 107, 10490–10495.
Ikegami K, Setou M (2009). TTLL10 can perform tubulin glycylation when co-expressed with TTLL8. FEBS Lett 583, 1957–1963.
Jana SC, Marteil G, Bettencourt-Dias M (2014). Mapping molecules to structure: unveiling secrets of centriole and cilia assembly with near-atomic resolution. Curr Opin Cell Biol 26, 96–106.
Janke C *et al.* (2005). Tubulin polyglutamylase enzymes are members of the TTL domain protein family. Science 308, 1758–1762.
Janke C, Bulinski JC (2011). Post-translational regulation of the microtubule cytoskeleton: mechanisms and functions. Nat Rev Mol Cell Biol 12, 773–786.
Kalinina E, Biswas R, Berezniuk I, Hermoso A, Aviles FX, Fricker LD (2007). A novel subfamily of mouse cytosolic carboxypeptidases. FASEB J 21, 836–850.
Kimura Y, Kurabe N, Ikegami K, Tsutsumi K, Konishi Y, Kaplan OI, Kunitomo H, Iino Y, Blacque OE, Setou M (2010). Identification of tubulin deglutamylase among Caenorhabditis elegans and mammalian cytosolic carboxypeptidases (CCPs). J Biol Chem 285, 22936–22941.
Ko J, Park H, Heo L, Seok C (2012). GalaxyWEB server for protein structure prediction and refinement. Nucleic Acids Res 40, W294–W297.
Källberg M, Wang H, Wang S, Peng J, Wang Z, Lu H, Xu J (2012). Template-based protein structure modeling using the RaptorX web server. Nat Protoc 7, 1511–1522.
Lalle M, Camerini S, Cecchetti S, Blasetti Fantauzzi C, Crescenzi M, Pozio E (2011). Giardia duodenalis 14-3-3 protein is polyglycylated by a tubulin tyrosine ligase-like member and deglycylated by two metallocarboxypeptidases. J Biol Chem 286, 4471–4484.
Laskowski RA (2001). PDBsum: summaries and analyses of PDB structures. Nucleic Acids Res 29, 221–222.
Ludueña R, Banerjee A (2008). The isotypes of tubulin: distribution and functional significance. In: The Role of Microtubules in Cell Biology, Neurobiology, and Oncology, ed. T Fojo, Totowa, NJ: Humana Press, 123–175.
Luthy R, Bowie JU, Eisenberg D (1992). Assessment of protein models with three-dimensional profiles. Nature 356, 83–85.
Lyons PJ, Fricker LD (2011). Carboxypeptidase O is a glycosylphosphatidylinositol-anchored intestinal peptidase with acidic amino acid specificity. J Biol Chem 286, 39023–39032.
Otero A, Rodríguez de la Vega M, Tanco S, Lorenzo J, Avilés FX, Reverter D (2012). The novel structure of a cytosolic M14 metallocarboxypeptidase (CCP) from Pseudomonas aeruginosa: a model for mammalian CCPs. FASEB J 26, 3754–3764.
Pathak N, Austin-Tse Ca, Liu Y, Vasilyev A, Drummond Ia (2014). Cytoplasmic carboxypeptidase 5 regulates tubulin glutamylation and zebrafish cilia formation and function. Mol Biol Cell 25, 1836–1844.
Paturle-Lafanechère L, Eddé B, Denoulet P, Dorsselaer, Van A, Mazargui H, Le Caer JP, Wehland J, Job D, Van Dorsselaer A, *et al.* (1991). Characterization of a major brain tubulin variant which cannot be tyrosinated. Biochemistry 30, 10523–10528.
Paturle-Lafanechère L, Manier M, Trigault N, Pirollet F, Mazarguil H, Job D (1994). Accumulation of delta 2-tubulin, a major tubulin variant that cannot be tyrosinated, in neuronal tissues and in stable microtubule assemblies. J Cell Sci 107, 1529–1543.
Redeker V, Levilliers N, Schmitter JM, Le Caer JP, Rossier J, Adoutte A, Bré MH (1994). Polyglycylation of tubulin: a posttranslational modification in axonemal microtubules. Science 266, 1688–1691.
Rocha C, Papon L, Cacheux W, Marques Sousa P, Lascano V, Tort O, Giordano T, Vacher S, Lemmers B, Mariani P, *et al.* (2014). Tubulin glycylases are required for primary cilia, control of cell proliferation and tumor development in colon. EMBO J, e201488466.
Rodriguez de la Vega M, Sevilla RG, Hermoso A, Lorenzo J, Tanco S, Diez A, Fricker LD, Bautista JM, Avilés FX (2007). Nna1-like proteins are active metallocarboxypeptidases of a new and diverse M14 subfamily. FASEB J 20, 851–865.
Rodríguez de la Vega Otazo M, Lorenzo J, Tort O, Avilés FX, Bautista JM (2013). Functional segregation and emerging role of cilia-related cytosolic carboxypeptidases (CCPs). FASEB J 27, 424–431.
Rogowski K, Juge F, van Dijk J, Wloga D, Strub JM, Levilliers N, Thomas D, Bré MH, Van Dorsselaer A, Gaertig J, *et al.* (2009). Evolutionary divergence of enzymatic mechanisms for posttranslational polyglycylation. Cell 137, 1076–1087.
Rogowski K, van Dijk J, Magiera MM, Bosc C, Deloulme JC, Bosson A, Peris L, Gold ND, Lacroix B, Bosch Grau M, *et al.* (2010). A family of protein-deglutamylating enzymes associated with neurodegeneration. Cell 143, 564–578.
Roy A, Kucukural A, Zhang Y (2010). I-TASSER: a unified platform for automated protein structure and function prediction. Nat Protoc 5, 725–738.
Sahab ZJ, Hall MD, Me Sung Y, Dakshanamurthy S, Ji Y, Kumar D, Byers SW (2011). Tumor suppressor RARRES1 interacts with cytoplasmic carboxypeptidase AGBL2 to regulate the α-tubulin tyrosination cycle. Cancer Res 71, 1219–1228.
Schechter I, Berger A (1967). On the size of the active site in proteases. I. Papain. Biochem Biophys Res Commun 27, 157–162.
Shang Y (2002). Tetrahymena thermophila contains a conventional gamma-tubulin that is differentially required for the maintenance of different microtubule-organizing centers. J Cell Biol 158, 1195–1206.
Sippl MJ (1993). Recognition of errors in three-dimensional structures of proteins. Proteins 17, 355–362.
Sirajuddin M, Rice LM, Vale RD (2014). Regulation of microtubule motors by tubulin isotypes and post-translational modifications. Nat Cell Biol 16, 335–344.
Thompson WC (1977). Post-translational addition of tyrosine to alpha tubulin in vivo intact brain and in myogenic cells in culture. FEBS Lett 80, 9–13.
Van Dijk J, Rogowski K, Miro J, Lacroix B, Eddé B, Janke C (2007). A targeted multienzyme mechanism for selective microtubule polyglutamylation. Mol Cell 26, 437–448.
Vogel P, Hansen G, Fontenot G, Read R (2010). Tubulin tyrosine ligase-like 1 deficiency results in chronic rhinosinusitis and abnormal development of spermatid flagella in mice. Vet Pathol 47, 703–712.
Wei S, Segura S, Vendrell J, Aviles FX, Lanoue E, Day R, Feng Y, Fricker LD (2002). Identification and characterization of three members of the human metallocarboxypeptidase gene family. J Biol Chem 277, 14954–14964.
Wiederstein M, Sippl MJ (2007). ProSA-web: interactive web service for the recognition of errors in three-dimensional structures of proteins. Nucleic Acids Res 35, W407–W410.
Wloga D, Rogowski K, Sharma N, Van Dijk J, Janke C, Eddé B, Bré MH, Levilliers N, Redeker V, Duan J, *et al.* (2008). Glutamylation on α-tubulin is not essential but affects the assembly and functions of a subset of microtubules in Tetrahymena thermophila. Eukaryot Cell 7, 1362–1372.
Wu H-Y, Wang T, Li L, Correia K, Morgan JI (2012). A structural and functional analysis of Nna1 in Purkinje cell degeneration (pcd) mice. FASEB J 26, 4468–4480.
Zhang Y (2008). I-TASSER server for protein 3D structure prediction. BMC Bioinformatics 9, 40.

Supplemental Materials

Molecular Biology of the Cell

Tort et al.

Supplemental Material

Supplemental figure legends

Figure S1. Structural alignment of CCPs and determination of amino acids of the active site. A) Structural alignment of the catalytic domain of hCCP3 with the CCP crystal structures of *Pseudomonas aeruginosa* (PDB 4a37) (Otero *et al.*, 2012), *Burkholderia mallei* (PDB 3k2k) and *Shewanella denitrificans* (PDB 3l2n) obtained with the RaptorX server. **B)** Comparison of the amino acids shaping the S1' binding pocket in different carboxypeptidases with different defined amino-acid specificities. Residues are indicated following the RasMol amino color scheme that colors amino acids accordingly to their properties. [a]Residue 207 is the major determinant of specificity for M14B carboxypeptidases. [b]Residue 255 is the major determinant of specificity for M14A carboxypeptidases. [c]Carboxypeptidase isolated from *Thermoactinomyces vulgaris* that is a model for broad substrate specificity. [d]M14D is the proposed classification for the M14 members that constitute the CCP subfamily. **C)** Amino acid sequence alignment of the region around position 255 of CCPs and canonical bovine CPA. The positions known to participate in the binding of the substrate C-terminal residue are indicated.

Figure S2. Sequence optimization of active mCCP2 and mCCP3. To confirm that our truncated 65-kD versions of mCCP2 and mCCP3 (Figure 2A, B) represent the shortest active version of these enzymes, we further truncated short sequences at their N- and the C-termini. **A)** Scheme of full-length of mCCP6, mCCP2, mCCP3 and several truncated forms of mCCP2 and mCCP3. The green boxes indicate in the conserved N-terminal domain (Nt) specific to CCPs, the blue box is the conserved carboxypeptidase domain (CP; compare with Figure 2A). Carboxypeptidase domain schemes were delimitated with Superfamily 1.73 database (Gough *et al.*, 2001). Gray lines are non-conserved sequences that were partially truncated in the optimization. **B)** Immunoblot analysis HEK293T cell extracts expressing different forms of YFP-mCCP2 and YFP-mCCP3 as shown in (**A**). The deglutamylase activity is monitored by the generation of Δ2-tubulin. 12G10 is used to control α-tubulin loading. **C)** Secondary structure prediction of an essential C-terminal fragment determined in

mCCP2 and mCCP3 performed with Coils server (Lupas *et al.*, 1991). The fragment present in mCCP2_Z1703 and mCCP3_Z1670, but deleted in mCCP2_1607 and mCCP3_Z1583 has a high probability for coiled-coil structure. Coiled-coil structures are known to participate in structural stabilization and oligomerization of proteins (Parry *et al.*, 2008). It is thus possible that the removal of these coiled-coil sequences from mCCP2 and mCCP3 resulted in misfolded or destabilized enzymes, and consequently in loss-of-activity. Alternatively, it could indicate that both enzymes need to oligomerize for activity.

Figure S3. **Specificity tests for truncated mCCP2 and mCCP3.** Immunoblot analysis of HEK293T protein extracts co-expressing truncated forms of YFP-mCCPs and YFP-telokin variants. **A)** Co-expression of active or dead truncated forms of YFP-mCCP2 and YFP-mCCP3 together with YFP-telokin variants ending in different acidic tails to test their ability to release single of multiple Asp and/or Glu residues. Generation of the Δ2-tubulin epitope on telokin is used to monitor C-terminal degradation. mCCP1 is used as positive control for deglutamylation. Note that only mCCP3-Z1670 is efficiently removing single and consecutive Asp residues. See also Figure 3B. **B)** Epitope mapping of polyG antibody on artificial C-terminal tails of YFP-telokin with different numbers of Gly residues. Note that only poly-Gly chains of four and longer are recognized by this antibody. (*non-specific band recognized by the polyG antibody). **C)** Schematic representation of the experimental setup used to identify deglutamylation and deglycylation activities. YFP-telokin with 3-Glu tails (detected by polyE) or 4-Gly tails (detected with polyG) are co-expressed with YFP-CCPs. The immunoblots show that truncated versions of YFP-mCCP2 and YFP-mCCP3 efficiently remove C-terminal Glu residues thus extinguishing the polyE signal. In contrast, no change in the polyG signal was detected in the deglycylation test.

Figure S4. qRT-PCR analyses expression levels of mCCP1, mCCP4, mCCP5 and mCCP6 in murine tissues and analysis of *Agbl2* and *Agbl3* KO mice. A) Relative expression levels of mCCP1, mCCP4, mCCP5 and mCCP6 in different organs of 4-month-old wild type mice as determined by

qRT-PCR. Average values relative to the *Tbp* gene expression are represented, and error bars represent standard deviation of three to five independent experiments. Experiments are complementary to Figure 4A. Values are used for Figure 4B. **B)** Comparative immunoblot analysis of protein extracts from different organs of 5-weeks old wild type (WT) and *Agbl2* or *Agbl3* KO mice with polyE. Total tubulin levels were detected with anti-α-tubulin antibody (12G10). Note that a 130-kDa substrate shows increased polyE signals stomach of *Agbl2* or *Agbl3* KO mice, and in oviduct of the *Agbl3* KO mouse.

Figure S5. Analyses of the polyglutamylation levels in *Agbl2*/*Agbl3* double KO mice. A) Immuno blots of testes and sperm extracts from four of each, WT and *Agbl2*/*Agbl3* double KO mice (mice 1, 2, 3, 5, 6 and 7 were 4 months old; mice 4 and 8 were 5 weeks old). The polyE and 12G10 signals as represented here have been quantified using the software ImageJ, and polyE values have been adjusted to the total tubulin load detected with the antibody 12G10. Mean values have been plotted in Figure 4E. *Note that the 130-kDa polyE-positive protein band is only detected in the 5-week old mouse (which is shown in Figure 4D), but not in the older individuals.

Figure S6. Strategy for the generation of the knockout mice. Schematic representation in scale of the targeting vector used and all the possible alleles for *Agbl2* and *Agbl3* genes. Orange bar: genomic DNA. Black boxes: exons with their corresponding number. Green and purple arrowheads: LoxP and Flp sequences, respectively. White bar: *neo* cassette, with the neomycin resistance gene (white box). Blue lines: zone of sequence homology for homologous recombination, with the corresponding size in kbp. Black arrowheads: primers used for the PCR genotyping.

Supplemental Tables

Table S1. Primers used to clone or mutagenize CCP genes and their truncated forms.

Gene	Vector	Primers Fw/Rev
mCCP1	pcDNA3.1-EYFP	Fw: cgcggagtcgacACC ATGAGCAAGCTAAAAGTGGTGGGAGAG Rev: cgccgctgatca AATCAGGTGTGTTCTTGATACCTCAG
mCCP2	pEYFP	Fw: cgcggactcgagACC ATGAATGTCCTGCTTGAGATGGCTTTTC Rev: cgccgcagatct TGGGTATGTGTATATATGCAAGGATGGG
mCCP3	pEYFP	Fw: cgcggactcgagACC ATGTCAGAAGATTCAGAGGAGGAAGAC Rev: cgccgcggatcc CTGATGCTGTTGCAAGTTGGCTATC
mCCP3_opt	pEYFP	Synthetic gene optimized for bacterial codon usage (GeneCust).
hCCP3	pOPINFS	from N. Berrow (IRB, Barcelona, Spain)
mCCP4	pEGFP	Fw: cgaattctagccATGGCTGAACAAGAAGGCAGT Rev: ctggatccgggagacacagagatgtcac (non coding region)
mCCP5	pEYFPr	Fw: ccgcgactgcagACC ATGGAGCTGCGCTGTGGGGGATTGC Rev: ccgcgaggtacc TCCCTCTGCGAGTCGGCGGTGAGC
mCCP6	pEYFP	Fw: cgcggactcgagACC ATGGCGGAGCGGAGCCAGACAGCGCC Rev: ccgcagaTCT AAAGGGGGTTGATGGGTCTTTG
mCCP2_N2190	pEYFP	Fw: cgcggactcgagACC ATGAATGTCCTGCTTGAGATGGCTTTTC Rev: ccgcggatcc GCTCTTCTGGTACTGCTCATTCCG
mCCP2_N1992	pEYFP	Fw: cgcggactcgagACC ATGAATGTCCTGCTTGAGATGGCTTTTC Rev: ccgcggatcc TAAATCCATATCTTGTCCAAAGTTATTC
mCCP2_Z1703	pEYFP	Fw: cggactcgagACC atgGACTCACTTCTGCTGAGCTCGCC Rev: ccgcggatcc TAAATCCATATCTTGTCCAAAGTTATTC
mCCP2_Z1334	pEYFP	Fw: cggactcgagACC atgACACTGCAAGGGCCGGACGAC Rev: ccgcggatcc TAAATCCATATCTTGTCCAAAGTTATTC
mCCP2_Z1607	pEYFP	Fw: cggactcgagACC atgGACTCACTTCTGCTGAGCTCGCC Rev: ccgcggatcc GTCAGGATCACAGAAATCCAG
mCCP3_N1998	pEYFP	Fw: cggactcgagACC ATGAGCGAGGACTCTGAAGAAG Rev: ccgcggatcc GTAAACTTCCTGCATATTGTTCTGG
mCCP3_N1809	pEYFP	Fw: cggactcgagACC ATGAGCGAGGACTCTGAAGAAG Rev: ccgcggatcc GGTATCCGTGTTATCGGAGACGC
mCCP3_Z1670	pEYFP	Fw: cggactcgagACC atgGACCCGTTTTTCCCACGCACCAC Rev: ccgcggatcc GGTATCCGTGTTATCGGAGACGC
mCCP3_Z1325	pEYFP	Fw: cggactcgagACC atgGTGGATAACTGCGACAACACCC Rev: ccgcggatcc GGTATCCGTGTTATCGGAGACGC
mCCP3_Z1583	pEYFP	Fw: cggactcgagACC atgGACCCGTTTTTCCCACGCACCAC Rev: ccgcggatcc GTCCGGGTCGCAGTAGTCCAG
mCCP2_E593Q (dead version)	pEYFP	Fw: GCTACACCATGcAGTCTACCTTTGGC Rev: CAAAGGTAGACTgCATGGTGTAGCTG
mCCP3_E540Q (dead version)	pEYFP	Fw: CTTTCACCCTGcAAGCAACTTTCTGCG Rev: GAAAGTTGCTTgCAGGGTGAAAGAATTGC

Table S2. Primary antibodies used in this study

Antibody name	Antigen	Type	Dilutions			Provider
			immuno blot		immuno cyto-chemistry	
			cell lines	tissue extracts		
12G10	α-tubulin	mouse monoclonal	1:1,000	1:400	-	from J. Frankel, E. M. Nelson, University of Iowa, USA
anti-β-tubulin	β-tubulin	mouse monoclonal	-	-	1:200	Sigma #T5201
anti-Δ2-tubulin	CEGEEEGE-COOH	rabbit polyclonal	1:5,000	1:5,000	1:1,000	our own production
anti-deTyr-tubulin	-CGEEEGEE-COOH	rabbit polyclonal	1:2,000	-	-	Millipore #AB3201
polyE	-CEEEEEEEEE-COOH	rabbit polyclonal	1:4,000	1:10,000	-	our own production
polyG	-CGGGGGGGGG-COOH	rabbit polyclonal	1:6,000	-	-	our own production
anti-GFP	GFP, YFP, CFP	rabbit polyclonal	1:5,000	-	-	Torrey Pines Biolabs, #TP401

Table S3. Search for C-terminal acidic amino acid stretches

	Number of proteins with uninterrupted E/D-stretches at the C-terminus				
Organism	**2**	**3**	**4**	**5**	**6+**
Homo sapiens	287	60	16	12	24
Mus musculus	218	55	9	4	23
Drosophila melanogaster	47	9	2	3	6
Caenorhabditis elegans	42	14	6	3	4

	Number of proteins uninterrupted E-stretches at the C-terminus				
Organism	**2**	**3**	**4**	**5**	**6+**
Homo sapiens	94	12	1	1	3
Mus musculus	76	7	1	1	4
Drosophila melanogaster	14	1	0	0	2
Caenorhabditis elegans	16	0	0	0	2

Table S4. Primers used for qRT-PCR

Specificity	Gene	Primer name	Sequence (5'-3')
mouse	CCP1	AGTPBP1-U1	TTCCACAGAGTCAGATACTGCCAGAT
		AGTPBP1-L1	CAGAACTTCCATGCCTGTAGAACCT
	CCP2	AGBL2-U2	AATCTGCAGAAAGCCGTCAGAGT
		AGBL2-L2	AGTGTGTTTGTCCGTGTAGAGGTCA
	CCP3	AGBL3-U1	CTGTTTACCCAAACTCCAAGGAAGAT
		AGBL3-L1	GGATGTTCGGTTACCCCCAACT
	CCP4	AGBL1-U2	GAGCTGTCCTGTAGCTTTGAGGAACT
		AGBL1-L2	AAGCAACACTTGGAATGTGGTGGT
	CCP5	AGBL5-U2	GCACCCAAAAGGTCAGCCAT
		AGBL5-L2	GCCGCCTTCTGTCTGAGCA
	CCP6	AGBL4-U2	CCAAGAGTCTTTACCGAGATGGGAT
		AGBL4-L2	CTGTGGTCTGGGCAGCGATAGT

Supplemental References

Gough, J., Karplus, K., Hughey, R., and Chothia, C. (2001). Assignment of homology to genome sequences using a library of hidden Markov models that represent all proteins of known structure. J. Mol. Biol. *313*, 903–919.

Lupas, A., Dyke, M. Van, and Stock, J. (1991). Predicting coiled coils from protein sequences. Science *252*, 1162–1164.

Otero, A., Rodríguez de la Vega, M., Tanco, S., Lorenzo, J., Avilés, F. X., and Reverter, D. (2012). The novel structure of a cytosolic M14 metallocarboxypeptidase (CCP) from Pseudomonas aeruginosa: a model for mammalian CCPs. FASEB J. *26*, 3754–3764.

Parry, D. a D., Fraser, R. D. B., and Squire, J. M. (2008). Fifty years of coiled-coils and alpha-helical bundles: a close relationship between sequence and structure. J. Struct. Biol. *163*, 258–269.

A

```
3l2nA   1 P Y S Y E R H L D L I S A V Q - - - - L H P L V S T E H L G L T L D G R D M T L V K V G D D D P - - - 44
3k2kA   1 P Y S E E R H S E F L G A V Q - - - - Q M P Q A S V V E L G R T V E G R P M S L V V L G T P D - - - - 43
4a37A   1 P Y S R E R H A R L V E R A L - - - - G I E G V E R L A V G T S V Q G R D I E L L R V R R H P D - - - 44
hCCP3   1 P Y T Y T N L Q E Y L S G I N N D P V R S K F C K I R V L C H T L A R N M V Y I L T I T T P L K N S D 51

3l2nA  45 - - S K K S I W I T A R Q H P G E T M A E W L V E G L L N Q L L D - - - - N D C P T S K A L L D K A N 89
3k2kA  44 - - A K K K V W I I A R Q H P G E S M A E W F I E G L V K R L V G W G D W S G D P V A R K L Y D H A T 92
4a37A  45 - - S H L K L W V I A Q Q H P G E H M A E W F M E G L I E R L Q R - - - - P D D T E M Q R L L E K A D 89
hCCP3  52 S R K R K A V I L T A R V H P G E T N S S W I M K G F L D Y I L G - - - - - N S S D A Q L L R D T F V 97

3l2nA  90 F Y I V P N M N P D G S V R G H L R T N A V G A N L N R E W Q T P S L E R S P E V Y Y V V N K M H E T 140
3k2kA  93 F Y I V P N M N P D G S V H G N L R T N A A G A N L N R E W M E P D A E R S P E V L V V R D A I H A I 143
4a37A  90 L Y L V P N M N P D G A F H G N L R T N A A G Q D L N R A W L E P S A E R S P E V W F V Q Q E M K R H 140
hCCP3  98 F K V V P M L N P D G V I V G N Y R C S L A G R D L N R N Y T S L L K E S F P S V W Y T R N M V H R L 148

                                  K250                R255
3l2nA 141 - - - - G V D L F Y D V H G D E G L P Y V F L A G C E G I P N Y S D K L A S L Q Q D F V A A L S L A S 187
3k2kA 144 - - - - G C D L F F D I H G D E D L P Y V F A A G S E M L P G F T E Q Q R V E Q S A F I D S F K R A S 190
4a37A 141 - - - - G V D L F L D I H G D E E I P H V F A A G C E G N P G Y T P R L E R L E Q R F R E E L M A R G 187
hCCP3 149 M E K R E V I L Y C D L H G H S R K E N I F M Y G C D G S D R S - K T L Y L Q Q R I F P L M L S K N C 198
3l2nA 188 A D - F - - - Q T E F G Y D K D E P G K A N L T V A C N W V A N T F K C L S N T L E M P F K D N A N L 234
3k2kA 191 P D - F - - - Q D E H G Y P P G K Y R E D A F K L A S K Y I G H R F G C L S L T L E M P F K D N A N L 237
4a37A 188 - E - F - - - Q I R H G Y P R S A P G Q A N L A L A C N F V G Q T Y D C L A F T I E M P F K D H D D N 233
hCCP3 199 P D K F S F S A C K F N V Q K S K E G - - - - - T G R V V M W K M G I R N S F T M E A T F C G S T L G 244

3l2nA 235 A D P F Q G W S P E R S V Y F G E A S L I A M R A V I D K I G Q 266
3k2kA 238 P D E H I G W N G A R S A S L G A A M L G A I L E H V R A F - - 267
4a37A 234 P E P G T G W S G A R S K R L G Q D V L S T L A V L V D E L R - 264
hCCP3 245 N K R G T H F S T K D L E S M G Y H F C D S L L D Y C D P D R T 276
```

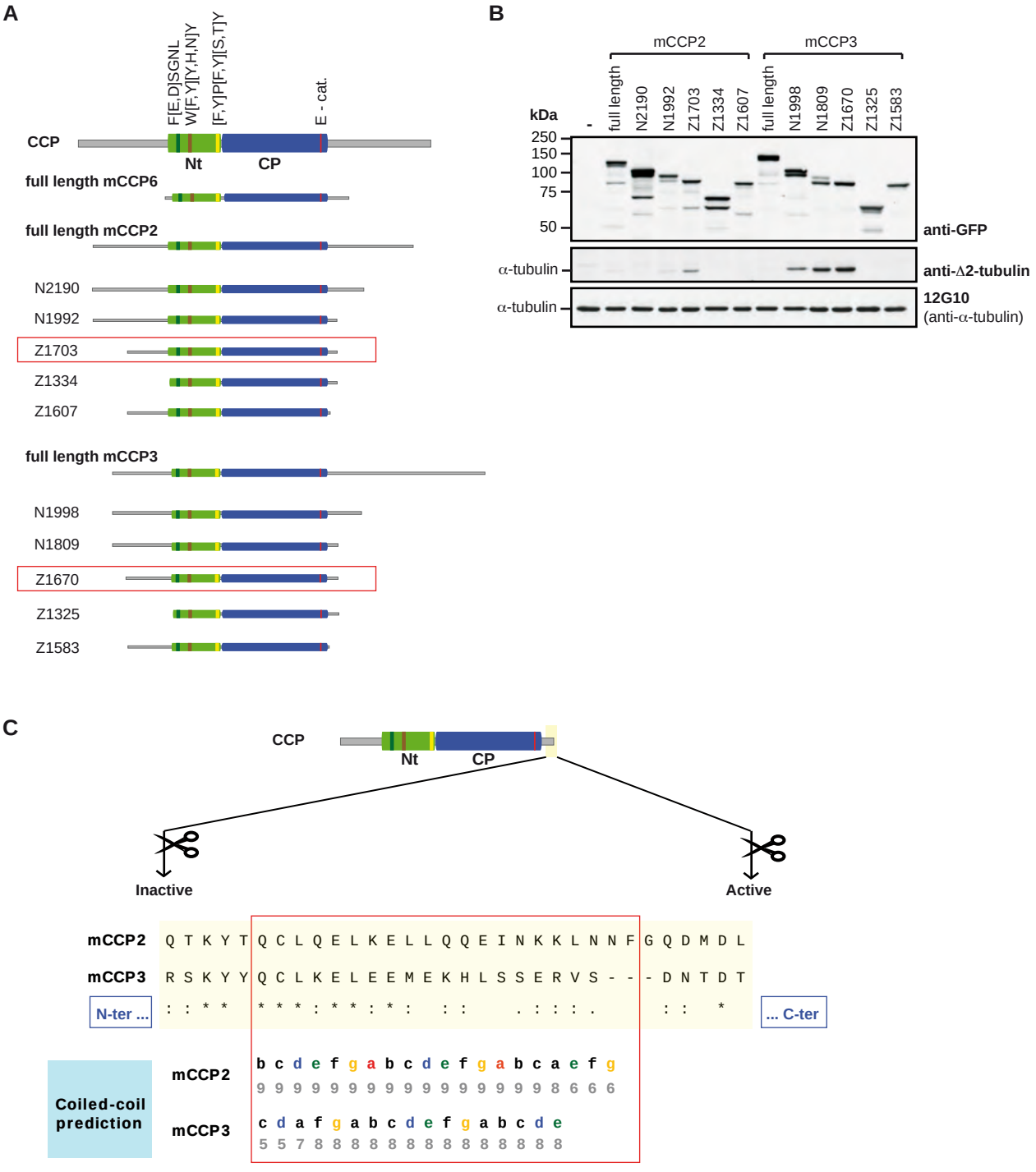
B

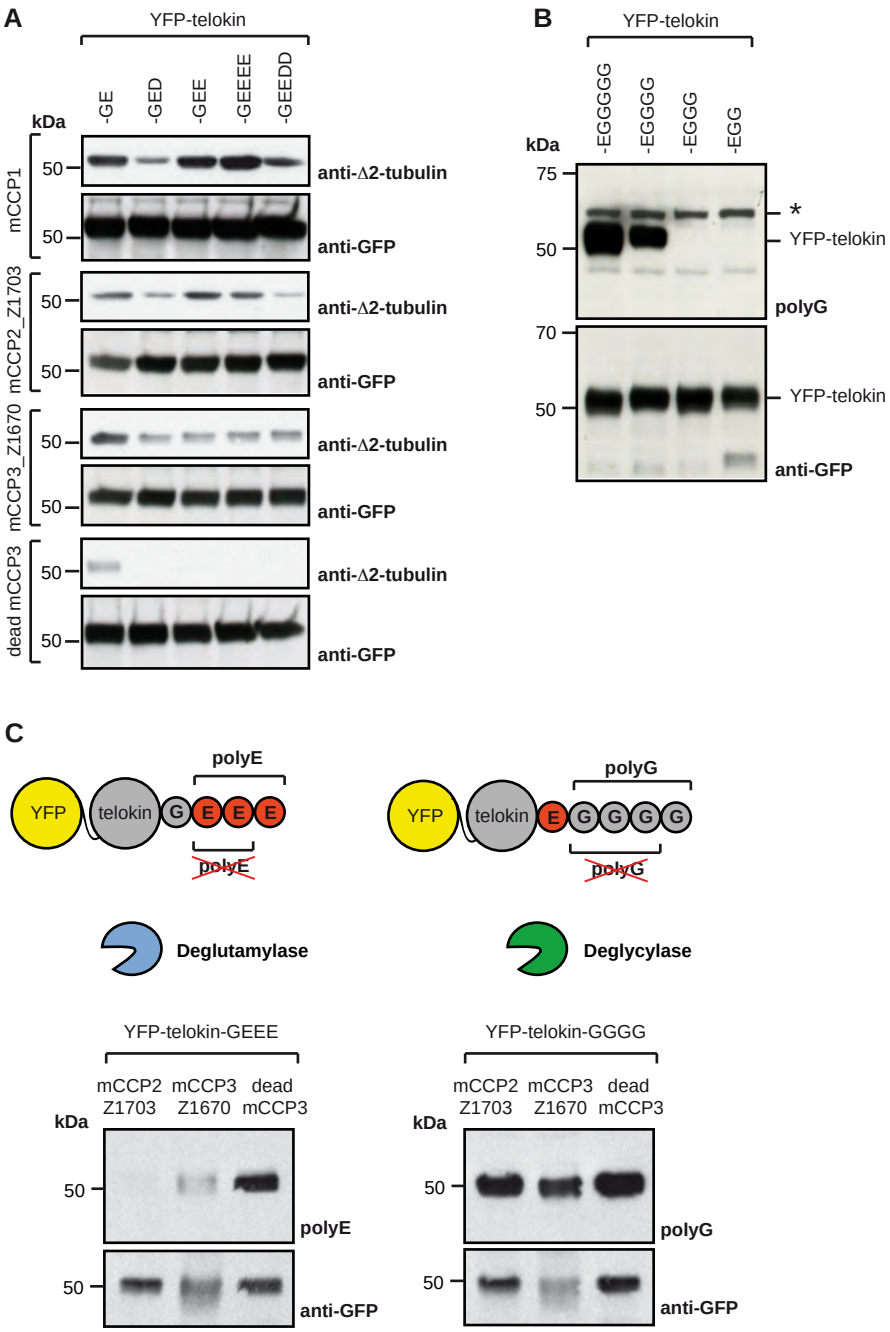
Position in bovine CPA (active form)	Homologous amino acid residues forming S1' subsite									Substrate specificity	MEROPS classification
	194	203	207[a]	243	247	250	253	255[b]	268		
Bovine CPA	Ser	Leu	Gly	Ile	Ile	Ala	Gly	Ile	Thr	Hydrophobic	M14A
Human CPA1	Ser	Met	Gly	Ile	Ile	Ala	Ser	Ile	Thr	Hydrophobic	
Human CPA2	Thr	Met	Gly	Ile	Ile	Ala	Gly	Ile	Ala	Hydrophobic	
Human CPA4	Asp	Met	Gly	Thr	Val	Ala	Ser	Ile	Thr	Hydrophobic	
CPT[c]	Thr	Leu	Gly	Gln	Leu	Thr	Asp	Thr	Thr	Broad	
Human CPB	Thr	Ile	Ser	Gly	Ile	Ala	Gly	Asp	Thr	Basic	
TAFI (CPU)	Ser	Val	Ser	Gly	Leu	Ala	Gly	Asp	Thr	Basic	
Human CPE	Asn	Asn	Asp	Gly	Trp	Val	Gly	Gln	Thr	Basic (Arg)	M14B
Human CPD	Asn	Asn	Asp	Asn	Phe	Val	Gly	Gln	Thr	Basic (Lys)	
Human CPO	Thr	Leu	Gly	Asn	Leu	Ser	Ser	Arg	Thr	Acidic	M14A
Human/ mouse CCP1	Asp	Val	Gly	Met	Ser	Lys	Thr	Arg	Thr	Acidic	M14D[d]
Human/ mouse CCP2	Asp	Val	Gly	Met	Ser	Arg	Thr	Arg	Thr	Acidic	
Human/ mouse CCP3	Asp	Ile	Gly	Phe	Asn	Lys	Thr	Arg	Thr	Acidic	
Human/ mouse CCP4	Asp	Ile	Gly	Phe	Lys	Lys	Thr	Arg	Thr	Acidic	
Human/ mouse CCP5	Asp	Cys	Gly	Phe	Asn	Lys	Ser	Arg	Thr	Acidic	
Human/ mouse CCP6	Asp	Gly	Gly	Tyr	Ser	Lys	Thr	Arg	Thr	Acidic	

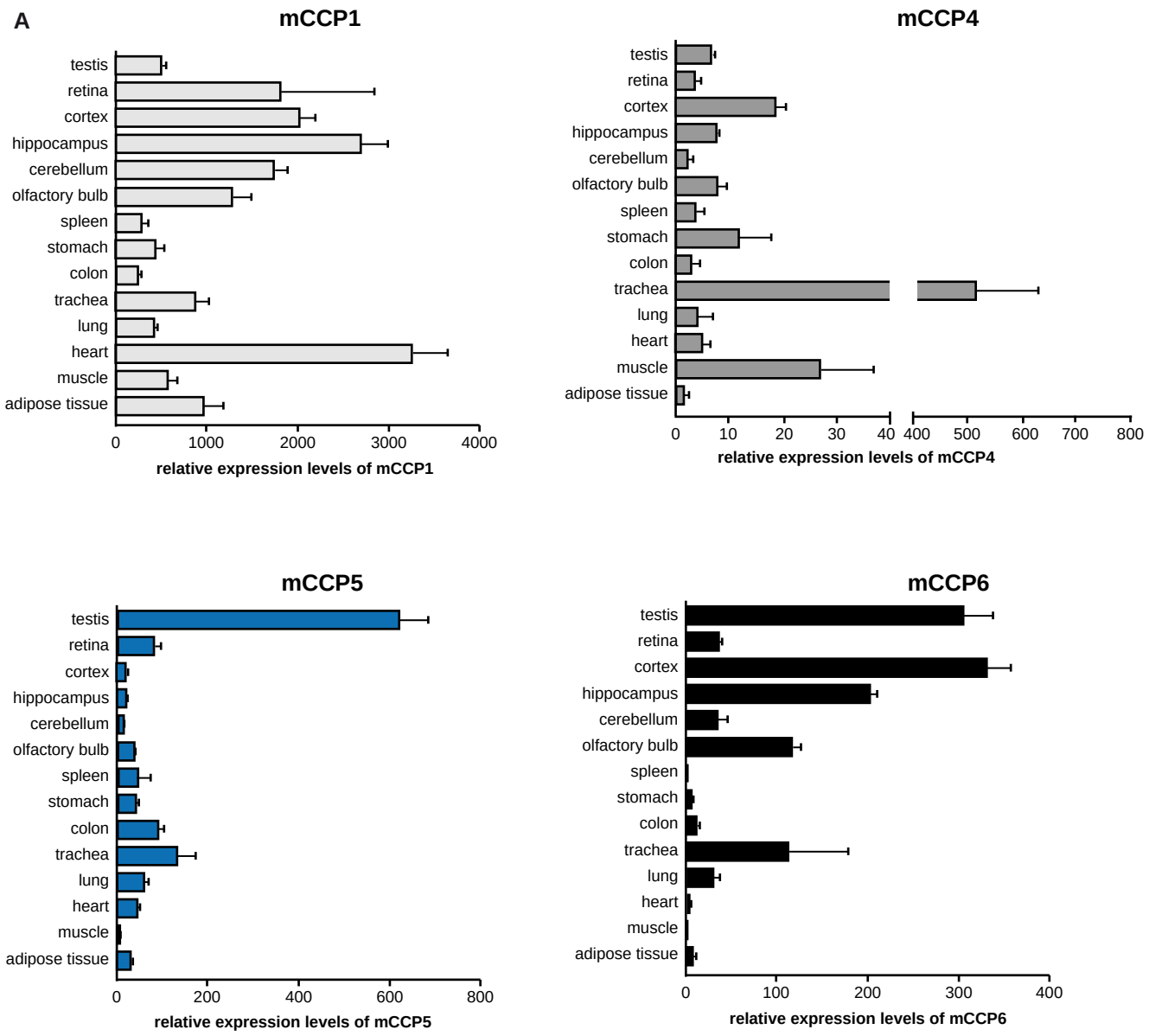
C

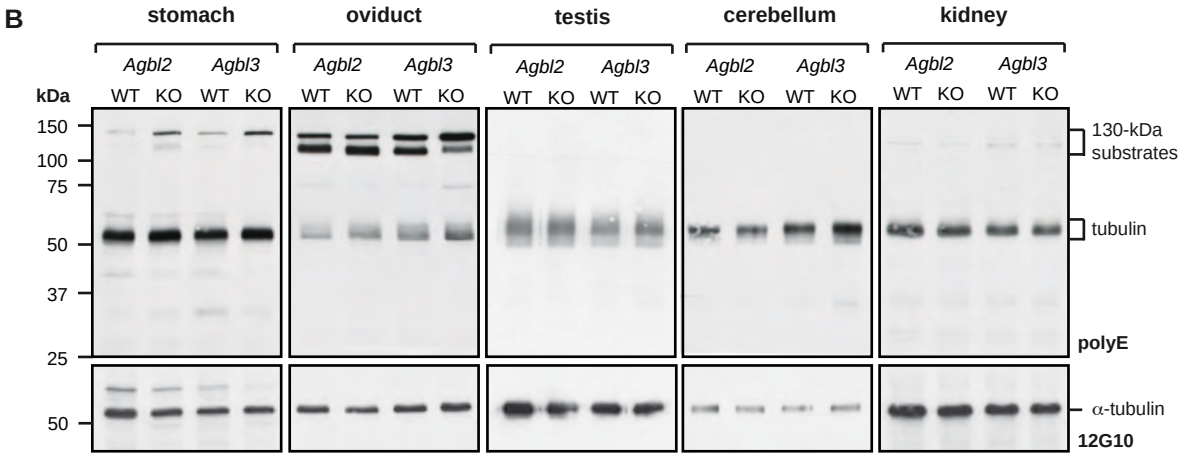
```
                  243 247                 250 253 255             268 270
CPA1_BOVIN  T-SYKYG-SIITTIYQ-------------ASGGSIDWSYNQ--GIKYSFTFELRDTGR
CCP1        I-APA-F-CMSSCSFVVEK----------SKESTAR VVVWREIGVQRSYTMESTLCGC
CCP4        L-APA-F-TMSSCSFLVEK----------SRASTAR-VVVWREMGVSRSYTMESSYCGC
CCP2        N-APDKF-SFHSCNFKVQK----------CKEGTGR-VVMWR-MGILNSYTMESTFGGS
CCP3        N-CPDKF-SFSACKFNVQK----------SKEGTGR-VVMWK-MGIRNSFTMEATFCGS
CCP5        N-SAH-F-DFQGCNFSEKNMYARDRRDGQSKEGSGR-VAIYKASGIIHSYTLECNYNTG
CCP6        N-AED-F-SYSSTSFNRDA----------VKAGTGRRFLGGLLDHTSYCYTLEVSFYSY
```

Tort et al., Supplementary Figure S2

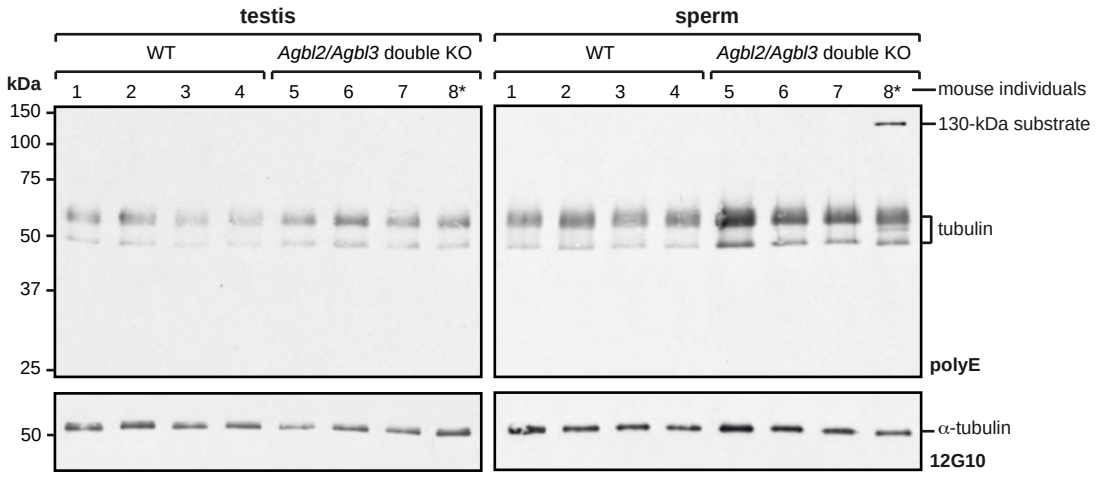



A
YFP-telokin
-GE
-GED
-GEE
-GEEEE
-GEEDD
kDa
mCCP1
mCCP2_Z1703
mCCP3_Z1670
dead mCCP3
50
anti-Δ2-tubulin
anti-GFP
B
YFP-telokin
-EGGGGG
-EGGGG
-EGGG
-EGG
kDa
75
70
50
*
YFP-telokin
polyG
anti-GFP
C
YFP
telokin
G
E
polyE
polyG
Deglutamylase
Deglycylase
YFP-telokin-GEEE
YFP-telokin-GGGG
mCCP2 Z1703
mCCP3 Z1670
dead mCCP3


A
mCCP1
testis
retina
cortex
hippocampus
cerebellum
olfactory bulb
spleen
stomach
colon
trachea
lung
heart
muscle
adipose tissue
0
1000
2000
3000
4000
relative expression levels of mCCP1
mCCP4
0
10
20
30
40
400
500
600
700
800
relative expression levels of mCCP4
mCCP5
0
200
400
600
800
relative expression levels of mCCP5
mCCP6
0
100
200
300
400
relative expression levels of mCCP6


B
stomach
oviduct
testis
cerebellum
kidney
Agbl2
Agbl3
WT
KO
kDa
150
100
75
50
37
25
50
130-kDa substrates
tubulin
polyE
α-tubulin
12G10

Tort et al., Supplementary Figure S5



Tort et al., Supplementary Figure S6

